



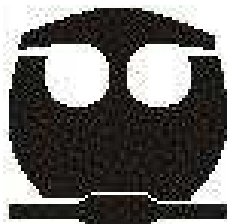
UNIVERSIDAD NACIONAL AUTÓNOMA DE
MÉXICO

FACULTAD DE QUÍMICA

"DISOLUCIÓN DE ARSENOPIRITA (FeAsS)
Y GALENA (PbS) EN PRESENCIA DE
DESFERRIOXAMINA-B A pH 5"

ACTIVIDAD DE INVESTIGACIÓN
QUE PARA OBTENER EL TÍTULO DE:

Q U Í M I C A
P R E S E N T A:
HILDA CORNEJO GARRIDO



MÉXICO, D. F.

2008



UNAM – Dirección General de Bibliotecas

Tesis Digitales
Restricciones de uso

DERECHOS RESERVADOS ©
PROHIBIDA SU REPRODUCCIÓN TOTAL O PARCIAL

Todo el material contenido en esta tesis está protegido por la Ley Federal del Derecho de Autor (LFDA) de los Estados Unidos Mexicanos (Méjico).

El uso de imágenes, fragmentos de videos, y demás material que sea objeto de protección de los derechos de autor, será exclusivamente para fines educativos e informativos y deberá citar la fuente donde la obtuvo mencionando el autor o autores. Cualquier uso distinto como el lucro, reproducción, edición o modificación, será perseguido y sancionado por el respectivo titular de los Derechos de Autor.

JURADO ASIGNADO:

PRESIDENTE	Profa. Norah Yolanda Barba Behrens
VOCAL	Prof. José de Jesus García Valdés
SECRETARIO	Profa. Javiera Cervini Silva
1 ^{er} SUPLENTE	Profa. Silvia Elena Castillo Blum
2 ^{do} SUPLENTE	Profa. Lilia del Carmen Lopez Serrano

Sitio donde se desarrolló el tema:

Laboratorio de Análisis Físicos y Químicos del Ambiente (LAFQA).
Instituto de Geografía. Universidad Nacional Autónoma de México

Dra. Javiera Cervini Silva
Asesora

M. en C. Ma. del Pilar Fernández Lomelín
Supervisor Técnico

Hilda Cornejo Garrido
Sustentante

ÍNDICE

PROTOCOLO DE INVESTIGACIÓN

1. INTRODUCCIÓN	1
2. OBJETIVOS	5
2.1 Objetivo general	
2.2 Objetivos particulares	
3. MATERIALES Y MÉTODOS	6
3.1 Materiales	
3.2 Métodos	
3.2.1 Tratamiento de las muestras minerales	
3.2.2 Experimentos de adsorción	7
3.2.3 Cuantificación del ligante DFO-B	
3.2.4 Cuantificación de Fe, As y Pb disueltos	8
3.2.5 Análisis superficial mediante MEB-EDS	
3.2.6 Especiación de arsénico	9
4 DISEÑO EXPERIMENTAL	
5 REVISIÓN BIBLIOGRÁFICA PRELIMINAR AL TEMA	11

ARTÍCULO

TITLE PAGE	14
ABSTRACT	15
INTRODUCTION	17
MATERIALS AND METHODS	21

RESULTS AND DISCUSSION	24
CONCLUSIONS	36
ACKNOWLEDGMENTS	38
TABLES	39
Table 1.	
Table 2.	40
Table 3.	41
FIGURES	42
Figure 1(a).	
Figure 1(b).	43
Figure 1(c).	44
Figure 1(d).	45
Figure 1(e).	46
Figure 2.	47
Figure 3.	48
Figure 4.	49
Figure 5.	50
Figure 6.	51
Figure 7.	52
Figure 8.	53
Figure 9.	54
Figure 10.	55
REFERENCES	56

1. INTRODUCCIÓN

Actualmente, el problema de contaminación ambiental a causa de metales y elementos tóxicos es de gran relevancia. Aunque la principal causa de contaminación por elementos tóxicos es debida a la intervención del hombre, existen procesos ambientales que inducen la movilización de dichos elementos en suelos, sedimentos, o cuerpos de agua. Un ejemplo de este fenómeno es el intemperismo, que se refiere al desgaste de minerales que ocurre debido a procesos físicos, químicos, o biológicos.

Por otro lado, son ampliamente conocidos los dos estados de oxidación del hierro; el hierro (II) que es la forma en la que encontramos al hierro en medios anaeróbicos, y el hierro(III), que está presente en medios aeróbicos, pero es menos soluble que el hierro (II). Gracias a esto, en entornos anaeróbicos no hay problema con la disponibilidad del hierro, pero la posibilidad de obtener hierro en condiciones aeróbicas es muy limitada (Kiss y Farkas, 1998). Dado que el requerimiento de hierro es necesario para casi todos los organismos, se tienen que buscar mecanismos alternos para acceder al hierro y así poder llevar a cabo los procesos biológicos necesarios para su supervivencia.

Un sideróforo¹ es un ligante biogénico de peso molecular relativamente bajo (generalmente menor a 1000 g/mol). La mayoría de los sideróforos actúan como ligantes hexadentados y agentes quelantes de metales pesados (Watteau and Berthelin, 1994; Hersman et al., 1995; Liermann et al., 2000; Maurice et al., 2000; Cocozza et al., 2002; Cervini-Silva and Sposito, 2002; Cheah et al., 2003; Kraemer et al., 2005; Haack et al., 2006). Sin embargo, son excepcionalmente efectivos en su especificidad para complejar Fe (III), la constante de afinidad es alrededor de 10^{30} M^{-1} (Wandersman and Delepeaire, 2004). Una de los sideróforos más comunes es la

¹ Del griego [σιδηρος (hierro)+ φερω(llevar)]

desferrioxamina-B (Figura 1) y es el sideróforo que se utilizó para realizar nuestros estudios.

Los sideróforos son sintetizados por una gran variedad de plantas y microorganismos (bacterias y hongos), son secretados como respuesta a la disminución en la disponibilidad de hierro soluble en suelos, sedimentos, y cuerpos de agua. En sistemas naturales, la fuente principal de hierro es de origen mineral, y la interacción de sideróforos con superficies minerales induce a la solubilización de Fe(III).

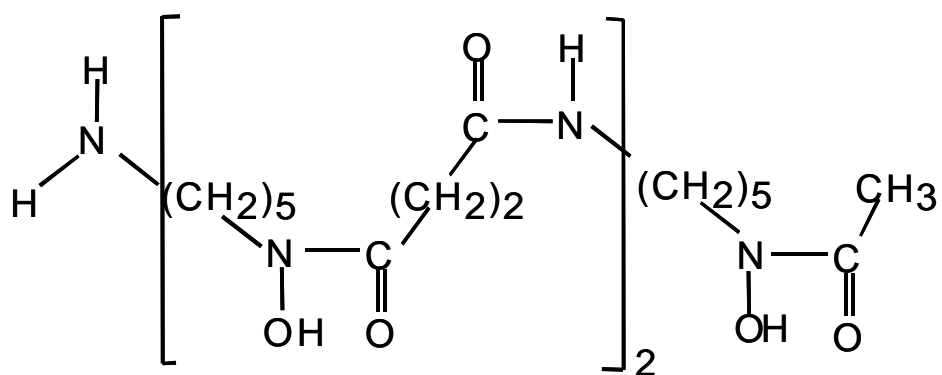


Figura 1. Estructura química del sideróforo desferrioxamina-B (DFO-B), producida por actinomicetos en el suelo.

En este trabajo, se realizó un estudio de la estabilidad de la Arsenopirita (FeAsS) -uno de las fuentes naturales más importantes de arsénico- y de la Galena (PbS), -la fuente natural más importante de plomo- en presencia de Desferrioxamina-B (DFO-B), un ligante sideróforo común, a pH 5.

Los resultados obtenidos muestran que la presencia del ligante biogénico incrementa el efecto de disolución de Fe y As presentes en la matriz de FeAsS . Además, se observa un incremento notable en la disolución de plomo elemental encontrado como impureza en la FeAsS .

Se realizaron experimentos de disolución de FeAsS a una concentración inicial de 1 g L^{-1} en presencia de DFO-B $200 \mu\text{M}$ a un pH inicial (pH_0) de 5 a distintos tiempos de agitación que van desde 1 h

hasta 110 h a 150 rpm. Para el caso de arsenopirita, en presencia de DFO-B 200 μ M, se observó un incremento en la disolución de Fe, As y Pb (a 110 h de exposición al ligante se encontraron valores de 0.4 ± 0.006 , 0.27 ± 0.009 y 0.14 ± 0.005 ppm, respectivamente) mientras que en los blancos de reacción la disolución de dichos elementos es menor (0.09 ± 0.004 , 0.15 ± 0.003 , y 0.01 ± 0.01 ppm, respectivamente). Dado que el efecto de disolución observado en las trazas de Pb presentes en la FeAsS fue mayor al presentado por Fe y por As, se realizaron experimentos en las mismas condiciones de reacción utilizando galena como posible donador de Pb soluble.

Aunque la diferencia entre la cantidad de plomo disuelto entre las muestras expuestas a agua y las muestras expuestas a DFO-B 200 μ M para el caso de la galena no fue tan dramática como lo fue para el caso del plomo elemental presente en la FeAsS, aun así tenemos que mencionar que se observa un incremento en la disolución de Pb cuando se tiene presente el ligante biogénico (a 110h de agitación, la cantidad de plomo disuelto en presencia de DFO-B 200 μ M fue de 35.66 ± 2.66 ppm, mientras que para los blancos, la cantidad de plomo disuelto fue de 21.8 ± 2.38 ppm).

Los análisis de MEB-EDS nos sugieren que a la par del efecto de disolución de la arsenopirita, en la superficie mineral se precipita azufre elemental.

Adicionalmente, se realizó el análisis de la especiación de As, para saber si hay una variación de las especies As(III)/As(V) a lo largo de la reacción de disolución en presencia de DFO-B y compararla con la reacción que se lleva a cabo en presencia de agua solamente, los resultados obtenidos muestran que la especie dominante en ambos casos, a tiempos de reacción menores a 30 horas es el As(V) (alrededor de 50-70%), a tiempos mayores de 30 horas, la especie dominante es As(III) en ambos tipos de condiciones de reacción, los resultados obtenidos difieren mucho a lo que se podría esperar, ya

que una vez que el As(III) se oxida a As(V), es muy difícil que éste se vuelva a reducir a As(III). Esto sugiere en primera instancia, que el mecanismo de oxido-reducción que se lleva a cabo es independiente de la presencia del ligante biogénico.

Finalmente, podemos decir que la importancia de este estudio radica en poder establecer un posible mecanismo natural que afecta al medio ambiente, ya que sugiere que un metal tan peligroso como lo es el plomo, así como un metaloide como el As se obtengan en forma soluble y disponible para los seres vivos.

2. OBJETIVOS

2.1 Objetivo General

El principal interés para este estudio es observar el efecto de disolución inducido por el ligante Desferrioxamina-B a los minerales arsenopirita (FeAsS) y galena (PbS) a pH_0 5.

2.2 Objetivos Particulares

- Encontrar las condiciones óptimas en cuanto al tamaño de partícula y tiempo de exposición de los minerales para obtener la máxima concentración de As y Pb disueltos.
- Proporcionar un posible mecanismo que sugiera el efecto de la desferrioxamina-B en la superficie mineral de la FeAsS , para lo cual se tomarán en cuenta otros factores como el cambio de pH y el cambio de la concentración de oxígeno disuelto en la solución.
- Caracterizar la superficie mineral de la arsenopirita antes y después de su exposición al ligante biogénico mediante Microscopía Electrónica de Barrido (MEB) acoplado a Espectroscopia de dispersión de Energía (EDS).
- Cuantificación de la cantidad de Fe, As, y Pb disueltos después de la exposición de la arsenopirita y la galena al ligante sideróforo.

3. MATERIALES Y MÉTODOS

3.1 Materiales

- El espécimen de arsenopirita utilizado para nuestros experimentos fue extraído de las minas de Panasqueira, Portugal, y fue comprado a Ward's Natural Science Establishment, Inc.
- La galena utilizada fue obtenida mediante una donación de la Colección Mineralógica del Museo de Geología de la Universidad Nacional Autónoma de México.
- El ligante sideróforo utilizado para nuestros experimentos fue el Mesilato de Desferrioxamina-B $[C_{25}H_{46}N_5O_8NH_3^+(CH_3SO_3^-)]$, adquirido de Sigma-Aldrich.
- Los estándares de Fe, As, y Pb (1000 mgL^{-1}) para Espectrometría de Absorción Atómica fueron comprados a Merck KGaA.

3.2 Métodos

3.2.1 Tratamiento de las muestras minerales

Antes de llevar a cabo los experimentos de disolución, las muestras minerales fueron lavadas con HCl 6 N, secadas y molidas en un mortero de ágata a un tamaño de partícula de 100-149 μm . El lavado con HCl se realizó para quitar “posibles” impurezas presentes en la superficie de los minerales. Varios autores sugieren utilizar un tamaño de partícula menor a 100 μm para favorecer el efecto de disolución en las superficies minerales, tras varios experimentos a tamaños de partículas menores, nos dimos cuenta que las partículas del mineral quedaban suspendidas en la superficie del frasco vial y el papel parafilm utilizado para sellar los viales, lo cual facilitaba la pérdida del material e incrementaba las variaciones entre nuestros

resultados. Es por esta razón que se utilizó un tamaño de partícula un poco mayor.

3.2.2. Experimentos de adsorción

La adsorción de la DFO-B a la superficie de las muestras minerales se realizó a pH₀ 5 y a temperatura ambiente. Se prepararon muestras con una concentración de 1 gL⁻¹ (1 g de mineral por 1 L de solución), el volumen total de cada muestra fue de 4 mL y se colocaron en viales de vidrio de una capacidad de 4 mL.

Se utilizaron dos distintos medios de reacción, el medio (A) que contenía DFO-B 200 µM y el medio (B) que corresponde a los blancos de reacción utilizando agua desionizada como medio de reacción. Para ajustar el pH a 5 de los 2 distintos medios se utilizó HCl 0.1 M (alrededor de 1 µL por muestra). Todas las muestras se realizaron por triplicado.

Posteriormente, las muestras se sometieron a agitación, para lo cual se utilizó un agitador Orbital Lab-Line Instruments modelo 4690 a una velocidad de 150 rpm. El tiempo de reacción de las muestras varió de 1 hasta 110 horas de agitación.

Al terminar el tiempo de agitación, las muestras fueron separadas con ayuda de jeringas BD 22 G X 32 mm.

3.2.3 Cuantificación del ligante DFO-B

Se utilizó un método colorimétrico para llevar a cabo la cuantificación del ligante que no reaccionó con el mineral después del tiempo de exposición (Solinas, 1994). Para lo cual se utilizó un espectrofotómetro UV/Vis marca Varian, modelo Cary 3E. A cada una de las muestras se le agregó un exceso de Fe(III), para lo cual se utilizó una solución de FeCl₃. Las muestras fueron acidificadas con HCl 6M antes de ser analizadas (se adicionó alrededor de 1 µL por

muestra para obtener un pH de 1.5-1.7). Las determinaciones colorimétricas se realizaron 2 horas después de haber adherido el exceso de Fe(III). La curva de calibración se realizó a una $\lambda_{\text{max}}=434\text{nm}$.

3.2.4 Cuantificación de Fe, As y Pb disueltos

Las soluciones obtenidas a los distintos intervalos de tiempo de exposición fueron analizadas mediante espectroscopia de absorción atómica utilizando un equipo SpectrAA 110 VGA 77, marca Varian, (equipado con una flama oxidante de aire-acetileno, AAS-F) con un SBW de 0.2nm y una lámpara de 5 mA. Para el caso de Fe y Pb, las lecturas fueron realizadas a una longitud de onda de 248.3 y 217.0 nm, respectivamente. El límite de detección de Fe fue de 0.02 mgL^{-1} , mientras que para Pb fue 0.033 mgL^{-1} .

Para las determinaciones de As se acopló un generador de hidruros marca Varian, HG, modelo VGA 77 a una longitud de onda de 193.7 nm. La generación de hidruros fue obtenida al mezclar una solución 8 M de HCl y una solución al 0.6 % de NaBH₄ disuelta en 0.5 % de NaOH. La reducción del arsénico total a As (III) de las muestras se logró adicionando KI al 20 %. El límite de detección experimental fue de $0.25 \mu\text{gL}^{-1}$.

3.2.5 Análisis superficial mediante MEB-EDS

Se realizó el análisis superficial a distintas muestras de FeAsS antes y después de ser expuestas al proceso de disolución mediante microscopía electrónica de barrido (MEB) utilizando un equipo marca Cambridge-Leica Stereoscan 440 y la composición química de las muestras fue obtenida utilizando un equipo de Espectroscopía de Dispersión de Energía (EDS) modelo Pentafet acoplado a MEB. Las muestras que fueron analizadas mediante MEB-EDS fueron tratadas

con (A) agua desionizada a $\text{pH}_0=5$ y (B) en presencia de DFO-B 2mM, a 95 y 430 h de agitación a 150 rpm.

3.2.6 Especiación de arsénico

La especiación de As (III) y As (V) se realizó mediante el acoplamiento de las técnicas de Cromatografía de Líquidos de Alta Definición (HPLC) y Espectrofotometría de Absorción Atómica (EAA) tomando como base el método descrito por Georgiadis et. al. (2006). Para la parte de HPLC se utilizó un equipo Solvent Dellivery System 9012 marca Varian con una columna de intercambio aniónico marca Bellefonte, modelo Supelcosil LC-SAX-1., mientras que para la parte de EAA se utilizó un equipo marca Varian, modelo SpectrAA. El método consiste en utilizar una fase móvil compuesta por un buffer de fosfatos 1.5 mM a un pH de 5.8 con un flujo de 2 mL min^{-1} a través de la columna de intercambio aniónico. Posteriormente, cuando la solución que contenía el As llegaba al espectrofotómetro de absorción atómica era tratado con HCl 10M y NaBH_4 al 0.6% para formar la arsina y así ser detectada.

4. DISEÑO EXPERIMENTAL

Para la realización de todos los experimentos de disolución, primeramente se seleccionó un tamaño de partícula de mineral adecuado para llevar a cabo los experimentos, para lo cual, en experimentos pioneros, se utilizaron tamaños de partícula mayores y menores, dando resultados más reproducibles los realizados con un tamaño de partícula entre 0.1-0.145 μm , el lavado ácido de los minerales utilizados se realizó con el fin de eliminar posibles impurezas presentes en la superficie del mineral.

La concentración inicial del mineral en el medio de reacción (1g de mineral por 1 L de solución), el $\text{pH}_0=5$, así como la temperatura

ambiente en el medio de reacción, se seleccionaron pensando en emular las condiciones normales del suelo.

Una vez establecidas las condiciones iniciales de las reacciones de disolución, se realizaron exposiciones de las muestras minerales a distintos tiempos de reacción que van desde 1 h hasta 110h, con la finalidad de observar como se va llevando a cabo el proceso de dilución, y de esta manera poder establecer si es un mecanismo que se lleva a cabo en sus primeras horas o si se va realizando de manera gradual a lo largo del tiempo.

Para poder establecer el tipo de mecanismo que se lleva a cabo, se retiraron muestras a determinados tiempos de reacción y se les realizó una cuantificación de la cantidad de ligante biogénico que había reaccionado, así como la cuantificación de la cantidad de Fe y As solubilizado. Al llegar a 110 h de reacción ya no se observó un incremento significativo en la cantidad de Fe disuelto, así que se decidió tomar a este tiempo como el último de nuestras mediciones.

Posteriormente se realizaron los análisis superficiales de la FeAsS con MEB-EDS con la finalidad de poder observar patrones de erosión o desgaste, los cuales nos sugirieron el efecto de disolución, la cuantificación de las proporciones de los distintos componentes de la matriz de FeAsS se realizó para poder establecer si había una precipitación de azufre elemental en la superficie de reacción posterior a la disolución del Fe y el As.

Los análisis de especiación de As se realizaron para poder determinar si había un cambio en el estado de oxidación inicial del As y de ser así, si este se volvía más o menos tóxico para el medio ambiente. Para poder justificar los resultados obtenidos en estas pruebas se midió la cantidad inicial y final del oxígeno disuelto de las muestras.

5. REVISIÓN BIBLIOGRÁFICA PRELIMINAR AL TEMA

Se han realizado muchos estudios para poder determinar la importancia de los ligantes sideróforos en el proceso de disolución de partículas naturales que representen una reserva primaria de hierro, por ejemplo, óxidos minerales y filosilicatos, como lo son la hematita (Hersman et al., 1995) y la hornblenda (Liermann et al., 2000).

También se ha estudiado la interacción de ligantes sideróforos en distintas arcillas como son la kaolinita (Maurice et al., 2001), o la esmectita (Haack et al., 2006).

Hay estudios acerca del efecto de disolución producido por sideróforos en algunos metales, por ejemplo Watteau and Berthelin, 1994; Maurice et al., 2000; Cheah et al., 2003, que estudiaron el efecto en aluminio.

En los experimentos iniciales con este ligante, utilizando como mineral a la goetita , Watteau and Berthelin (1994) demostraron la eficacia de la desferrioxamina-B para promover la disolución del hierro en comparación con otros ligantes biológicos comunes como el oxalato. Ellos atribuyen esta diferencia en disolución a la formación de un complejo específico habilitado por el ligante sideróforo. De manera similar, Kraemer et. al. (2005) reportaron un mayor efecto de disolución de Fe proveniente de goetita en la presencia de DFO-B, incluyendo la coordinación del sideróforo con un centro de Fe (III), presente en la superficie mineral como un precursor del proceso de disolución. Este paso mecanístico también fue sugerido por Holmen y Casey (1996), Holmen et. al. (1999) y por Kalinowski et. al. (2000) en sus estudios acerca de la cinética de la disolución mineral promovida por grupos hidroxamato.

Sin embargo no hay mucha información acerca del efecto de disolución que tienen los ligantes sideróforos en sistemas que contienen arsénico.

Se han realizado experimentos de disolución oxidativa de FeAsS, en presencia de oxígeno (Walker et. al., 2006) en donde se sugiere que la velocidad de oxidación de la arsenopirita es independiente de la cantidad de oxígeno presente. Steudel (1996); Cruz et. al. (1997) y Rohwerder et. al. (2003) proponen mecanismos de disolución de FeAsS inducida por medios ácidos, en donde se llega a la conclusión de que hay una precipitación de azufre elemental.

Finalmente, se sabe de estudios de disolución oxidativa de FeAsS inducida por la presencia de microorganismos como *Tiobacillus ferrooxidans* (Monroy-Fernandez et. al., 1995), en donde se llega a la conclusión de que la presencia de éste microorganismo facilita la disolución del mineral (posiblemente, debido a la presencia de sideróforos).

Por lo tanto, podemos llegar a la conclusión de que este es un estudio pionero que nos ayudará a determinar la influencia de ligantes sideróforos en minerales de gran importancia ambiental, provocando la contaminación de elementos elevadamente tóxicos como lo son el arsénico y el plomo.

Accepted Manuscript

Dissolution of Arsenopyrite (FeAsS) and Galena (PbS) in the Presence of Desferrioxamine-B at pH 5.

Hilda Cornejo-Garrido, Pilar Fernández-Lomelín, José Guzmán, Javiera Cervini-Silva

PII: S0016-7037(08)00095-1
DOI: [10.1016/j.gca.2008.02.008](https://doi.org/10.1016/j.gca.2008.02.008)
Reference: GCA 5563



To appear in: *Geochimica et Cosmochimica Acta*

Received Date: 16 October 2007
Accepted Date: 19 February 2008

Please cite this article as: Cornejo-Garrido, H., Fernández-Lomelín, P., Guzmán, J., Cervini-Silva, J., Dissolution of Arsenopyrite (FeAsS) and Galena (PbS) in the Presence of Desferrioxamine-B at pH 5., *Geochimica et Cosmochimica Acta* (2008), doi: [10.1016/j.gca.2008.02.008](https://doi.org/10.1016/j.gca.2008.02.008)

**Dissolution of Arsenopyrite (FeAsS) and Galena (PbS) in the
Presence of Desferrioxamine-B at pH 5.**

Hilda Cornejo-Garrido^{1,2}, Pilar Fernández-Lomelín²,
José Guzmán³, and Javiera Cervini-Silva^{2,*}

Geochimica et Cosmochimica Acta

(February 14, 2008)

Revised from

¹*Facultad de Química, Universidad Nacional Autónoma de México,
Cd. Universitaria, México D. F. CP 04510, México*

²*Instituto de Geografía, Universidad Nacional Autónoma de México,
Cd. Universitaria, México D. F. CP 04510, México*

³*Instituto de Investigación en Materiales, Universidad Nacional
Autónoma de México, Cd. Universitaria, México D. F. CP 04510,
México*

*Corresponding author:

Javiera Cervini-Silva

Instituto de Geografía, Universidad Nacional Autónoma de México
Circuito Exterior, Ciudad Universitaria, Coyoacán, Mexico City, 04510,
Mexico

Phone: 5622-4336, 5551-0880

Fax: +52 (5) 5616-2145

E-mail: jcervini@igg.unam.mx

Microorganisms and higher plants produce biogenic ligands such as siderophores to mobilize Fe that otherwise would be unavailable. In this paper we study the stability of arsenopyrite (FeAsS), one of the most important natural sources of arsenic on Earth, in the presence of desferrioxamine (DFO-B), a common siderophore ligand, at pH 5. Arsenopyrite specimens from mines from Panasqueira, Portugal (100–149 μm) that contained incrustations of Pb corresponding to elemental Pb, as determined by Scanning Electron Microscopy-Electron Diffraction Spectroscopy (SEM-EDX), were used for this study. Batch dissolution experiments of arsenopyrite (1 g L⁻¹) in the presence of 200 μM DFO-B at initial pH (pH_0) 5 were conducted for 110 h. In the presence of DFO-B, releases of Fe, As, and Pb showed positive trends with time; a shallower dependency was observed for release of Fe, As, and Pb in the presence of water only under similar experimental conditions. Detected concentrations of soluble Fe, As, and Pb in suspensions containing water only were found to be *ca.* 0.09 \pm 0.004, 0.15 \pm 0.003, and 0.01 \pm 0.01 ppm, correspondingly. In contrast, concentrations of soluble Fe, As, and Pb in suspensions containing DFO-B were found to be 0.4 \pm 0.006, 0.27 \pm 0.009, and 0.14 \pm 0.005 ppm, respectively. Notably, the effectiveness of DFO-B for releasing Pb was *ca.* ten times higher than that for releasing Fe. These results cannot be accounted for by thermodynamic considerations, namely, by size-to-charge ratio considerations proper of

metal complexation by DFO-B. As evidenced by SEM-EDX, elemental sample enrichment analysis supports the idea that the Fe-S subunit bond energy is limiting for Fe release. Likely, the mechanism(s) of dissolution for Pb incrustations is independent and occurs concurrently to that for Fe and As. Our results show that dissolution of arsenopyrite leads to precipitation of elemental sulfur, and is consistent with a non-enzymatic mineral dissolution pathway. Finally, speciation analyses for As indicate variability in the As(III)/As(V) ratio with time, regardless of the presence of DFO-B or water only. At reaction times < 30 h, As(V) concentrations were found to be 50-70%, regardless of the presence of DFO-B. These results are interpreted to mean that transformations of As are not imposed by ligand-mediated mechanisms. Experiments were also conducted to study the dissolution behavior of galena (PbS) in the presence 200 μ M at pH₀ 5. Results show that, unlike for arsenopyrite, the dissolution behavior of galena showed coupled increases in pH with decreases in metal solubility at $t > 80$ h. Oxidative dissolution mechanisms conveying sulfur oxidation bring about the production of {H⁺}. However, dissolution data trends for arsenopyrite and galena indicate {H⁺} consumption. It is plausible formation of Pb species dependent on {H⁺} and {OH⁻}, namely, stable surface hydroxyl complexes of the form Pb₄(OH)₄⁴⁺ (pH₅₀=5.8) and Pb₆(OH)₈⁴⁺ for pH values 5.8 or above.

INTRODUCTION

Arsenic (As) is widely distributed in nature (ca. $5 \times 10^{-4}\%$ earth's crust) (Voigt et al., 1996; Plant et al., 2005). Human beings are exposed to arsenic through food, water, and air. Depending on the route of exposure, inorganic arsenic brings about various health effects including stomach, intestine, and lung irritation, and skin damage. Ingestion of contaminated water containing inorganic arsenic can lead to cancer development, especially in the skin, lungs, liver, or bladder (Pinto and Nelson, 1976; Chen et al., 1985; Smith et al., 2002), and can contribute to a depletion in the production of red and white blood cells.

Arsenic can occur in the 5^+ , 3^+ , 0 , 1^- , and 2^- oxidation states in geological environments (Greenwood and Earnshaw, 1984). Mineral sources of arsenic include *arsenates* [containing As(V)O₄ units] (e.g., adelite [CaMgAsO₄(OH)], chalcophyllite [Cu₁₈Al₂(AsO₄)₃(SO₄)₃(OH)₂₇·3H₂O]); *arsenites* [containing As(III)O₃ units] (e.g., armangite [Mn₂₆(As₁₈O₅₀)(OH)₄CO₃], ecdemite [Pb₆As₂O₇Cl₄])); *elemental arsenic* [As(0)], *sulfides and arsenides* (e.g., arsenopyrite [FeAsS], lautite [CuAsS], skutterudite [(Cu, Ni)As₃]) and *sulfosalts* (e.g., orpiment [As₂S₃], realgar [AsS]) (Brown et al., 1999). In addition, arsenic can also be found as a minor or trace component in minerals (e.g., jarosite [KFe₃(SO₄)₂(OH)₆]). Arsenic is often found on rock surfaces combined with sulfur or metals, and arsenopyrite and orpiment are the earth's primary mineral sources of As.

The biogeochemical cycling of As is complex, driven by both natural processes such as mineral weathering (Nordstrom et al., 2003) and atmospheric deposition, and anthropogenic activities (Merian, 1991). High concentrations of As detected in geographical areas with no natural sources documented recently reveal the growing contribution of anthropogenic activities to As distribution (Nordstrom and Archer, 2003; O'Day et al., 2005). To add to the

complexity, the mobility and toxicity of As-bearing compounds vary with As oxidation state. For instance, As either as As(III) or As(V) forms anionic species when in aqueous solution, adsorbed to mineral surfaces, or incorporated into precipitates (Brown et al., 1999), yet As(V) adsorbs more strongly to mineral surfaces than does As(III), and thus is generally less mobile and potentially less bioavailable (Frost and Griffin, 1977; Korte and Fernando, 1991). In contrast, As(III)-bearing compounds are two to three times more toxic than As(V)-bearing compounds (Bottomley, 1984; Ng et al., 2003; Rodríguez et al., 2003), while reduced, inorganic As found in sulfide minerals is relatively low in toxicity. Oxidized inorganic As either as As(III) or As(V) compounds are significantly more toxic than many As organic complexes.

Of particular interest for this study is that biological activity instigates arsenopyrite dissolution. For example, incubations of arsenopyrite with *Thiobacillus ferrooxidans* under oxic conditions lead to the solubilization of Fe(III), As(III) and As(V) (Monroy-Fernández et. al., 1995) coupled with the formation of ferric arsenates and elemental sulfur. Comparable As and Fe release values were reported in arsenopyrite samples where bacterial attachment occurs and where it does not. Those results hint to the idea that bacterial attachment may not be limiting for mineral dissolution, and that it could also occur because of non-enzymatic pathways, possibly mediated by biogenic compounds such as organic ligands.

Organic ligands of small size and low molecular mass commonly found in soils, such as oxalate, enhance the dissolution of iron minerals (Cornell and Schwertmann, 2003). How organic ligands influence arsenopyrite dissolution remains largely unknown. To the authors' knowledge, there is little mechanistic work designed to study the non-enzymatic dissolution behavior of mineral arsenic. At circumneutral pH and 25°C, orpiment and realgar undergo oxidative dissolution (where dissolved oxygen serves as oxidant) (Lengke and

Tempel, 2002), involving the partial oxidation of structural arsenic and sulphur coupled with the formation of arsenates. The predominant As species in solution were arsenates as well as various sulphur species. Another study conducted in a/the Macraes (Craw et al., 2003) processing plant reports the oxidative dissolution of arsenopyrite. Observed concentrations of soluble As after seven-day exposure of arsenopyrite samples to oxidation and agitation were reported to be *ca.* 580 ppm in unsealed containers and *ca.* 140 ppm in sealed containers. Mineral dissolution was coupled with the precipitation of iron (hydr)oxides (Craw and Pacheco, 2002).

In oxic environments, such as highly weathered soils or surficial seawater, microorganisms and higher plants produce biogenic ligands such as siderophores to mobilize Fe that otherwise would be unavailable (Watteau and Berthelin, 1994; Hersman et al., 1995; Liermann et al., 2000; Maurice et al., 2000; Maurice et al., 2001; Cocozza et al., 2002; Cervini-Silva and Sposito, 2002; Cheah et al., 2003; Kraemer et al., 2005; Haack et al. 2006). Siderophore ligands can facilitate the dissolution of natural particles that represent a primary reservoir of iron, namely, oxide minerals and phyllosilicates including hematite (Hersman et al., 1995), hornblende (Liermann et al., 2000), unsubstituted (Cervini-Silva and Sposito, 2002; Cocozza et al., 2002; Kraemer et al., 2005) or aluminum (Watteau and Berthelin, 1994; Maurice et al., 2000; Cheah et al., 2003) goethite, and kaolinite (Maurice et al., 2001) or smectite (Haack et al. 2006) clay minerals.

Little quantitative information exists, however, on the dissolution of As-bearing minerals in the presence of siderophore ligands. In pioneering experiments with unsubstituted goethite, Watteau and Berthelin (1994) demonstrated the remarkable efficacy of the common trihydroxamate siderophore, desferrioxamine B (DFO-B), in promoting the solubilization of Fe, as compared to either protons or other common biological ligands, such as oxalate. They

attributed this difference to the Fe(III)-specific complexing ability of the siderophore ligands. Similarly, Kraemer et al. (2005) reported an enhanced rate of Fe release from goethite in the presence of DFO-B, concluding that coordination of the siderophore to an Fe(III) center at the mineral surface is a precursor to the dissolution process, a mechanistic step also suggested by Holmen and Casey (1996), Holmen et al. (1999) and by Kalinowski et al. (2000) in their studies of the kinetics of hydroxamate-promoted mineral dissolution. The objective of this study is an investigation of the dissolution behavior of arsenopyrite in the presence of DFO-B at pH 5.

MATERIALS AND METHODS

Materials. Specimens of arsenopyrite were extracted from mines in Panasqueira, Portugal, and purchased from Ward's Natural Science Establishment, Inc. Specimens of galena were obtained as gift from the Mineralogical Collection of the Museum of Geology, Universidad Nacional Autónoma de México.

Prior to use the mineral samples were prewashed with 6 N HCl, ground in an agate mortar, and sieved. Arsenopyrite samples with particle sizes between 100-149 µm were used for this study. Weathering report of AsSFe have been conducted using a particular size between 50-80 µm and pre washed AsSFe samples with 6N HCl (Monroy-Fernandez et al., 1995). We selected AsSFe samples bearing particular sizes between 100-149 µm. We observed in preliminary experiments that AsSFe samples in particle size would suspend in solution and stick to the vial water and cap which contribute to mass losses, therefore introducing error for quantifying metal release.

Determinations of specific surface area values were attempted by the static BET method. Experiments were conducted in triplicate.

Deionized water produced in a Barnstead Nanopure 4741 system (Iowa, USA; 17.7 MΩ cm) was used in all experiments. Containers and glassware were soaked overnight in 10% (v/v) nitric acid, then three-times washed and rinsed with deionized water prior to use. All chemicals were analytical grade.

Desferrioxamine B mesylate salt [$C_{25}H_{46}N_5O_8NH_3^+(CH_3SO_3^-)$] was purchased from Sigma-Aldrich (Italy). Sodium hydroxide pellets, hydrochloric acid 36.5-38%, Potassium iodide granular, nitric acid 70% and Sodium borohydride 98% were purchased from Mallinckrodt Baker (USA). Calibrations for atomic absorption spectrometric determinations were performed using commercial 1000 mg L⁻¹ arsenic, iron, and lead aqueous solutions purchased from Merck KGaA (Darmstadt, Germany).

SEM-EDX analyses. Arsenopyrite samples were reacted with 2 mM DFO-B at initial pH 5 for 95 and 430 h, stirred at 150 rpm. Surface analyses was obtained using a scanning electron microscopy. Chemical composition analyses of arsenopyrite samples were determined by energy dispersive spectroscopy. A Cambridge-Leica Stereoscan 440 Scanning Electron Microscope equipped with an Oxford, model Pentafet (EDX) was used. Backscattering electron micrographs were collected for all samples.

Dissolution experiments. Specimens of arsenopyrite were washed with 6 N HCl prior to use. The dissolution behavior of arsenopyrite was studied in the presence of (I) 200 μ M DFO-B solution and (II) water (blank). The initial pH (pH_0) for experimental conditions (I) and (II) was adjusted to 5 by adding aliquots of 0.01 N HCl solutions. Samples were placed in 4-mL Wheton-sample vials and placed in a stirrer (Orbital Lab-Line Instruments model 4690) at 150 rpm. All experiments were conducted in triplicate. Mineral suspensions were analyzed at various time intervals. Similar experiments were conducted to study the dissolution behavior of galena (PbS).

Adsorption experiments. Adsorption of DFO-B on arsenopyrite was investigated in batch mode at $pH_0 = 5$ with samples open to the atmosphere at room temperature. Specimens of arsenopyrite were placed in 4-mL Wheaton-sample vials. Aliquots of DFO-B stock solutions were then added to achieve the desired solution composition. The total volume of each sample was 4 mL, and the solids concentration adjusted to 1g L⁻¹. Mineral suspensions were equilibrated for 110 h at 150 rpm, then decanted. Aliquots of the supernatant solution were separated using a 22G x 32mm BD syringe needle.

The surface excess of DFO-B was calculated by dividing the concentration loss (initial concentration minus the total ligand concentration in the filtrate) by the solids concentration. Errors in

adsorbed concentration were estimated based on equating the sample coefficient of variation to the square root of the sum of squares of the coefficients of variation of constituent quantities in the definition of the surface excess.

Analytical techniques. Determinations for DFO-B concentration were conducted using a colorimetric method (Solinas, 1994) using a UV/VIS spectrophotometer (Varian, model Cary 3E) (CA, USA). Samples were acidified with 6 M HCl (*ca.* 1- μ L per sample) prior to analysis. pH values for all samples were 1.5 to 1.7. Colorimetric determinations were conducted 2 hr after adding Fe(III) excess. Spectral deconvolution for the determination of Fe-DFO-B concentration was determined using the minimum squared method for data acquired at $\lambda_{\text{max}} = 434$ nm in the presence of Fe(III) excess (as $\text{FeCl}_3 \cdot 6\text{H}_2\text{O}$; Solinas, 1994).

Determination of total soluble As, Fe, and Pb. Determinations of total soluble As were conducted using an atomic absorption spectrometer/AAS (Varian, SpectrAA 110, Melbourne, Australia) equipped with a hydride generator (HG, Varian, VGA 77) at 193.7 nm. Hydride generation was accomplished by mixing 8 M HCl and 0.6% NaBH_4 dissolved in 0.5% NaOH. Reduction of total As to As(III) in the standard or sample solutions was achieved by adding KI as described elsewhere (Elrick and Horowitz, 1986; Moffett, 1988). Experiments were conducted in triplicate. Negative blanks, internal standards, and certified materials were used in all experiments. The experimental detection limit for As was 0.25 ppb. The precision of the measurements was found to be within 0.5 – 1.5% RSD.

Determinations of total soluble Fe and Pb were conducted by atomic absorption spectrometry by using a Varian, SpectrAA 110 equipped with an acetylene-air oxidant flame (AAS-F) at 248.3 and 217.0 nm, respectively. Experimental detection limits were found to be 0.02 for Fe and 0.033 mg L⁻¹ for Pb.

Arsenic speciation. Speciation of As, namely As(III) and As(V), was conducted using an HPLC-AAS method described elsewhere (Georgiadis et al., 2006). Briefly, separation of As(III) and As(V) was conducted using an HPLC (Solvent Delivery System 9012, Varian, CA, USA) with a 100- μ L injection loop for sample introduction. This HPLC system was coupled with an AAS (SpectrAA 110, Varian, Mulgrave, Victoria, Australia). The mobile phase consisted of 1.5 mM phosphate at pH 5.8. The mobile phase was pumped isocratically at 2 mL min⁻¹ through an analytical anion exchange column (Supelcosil LC-SAX-1 Bellefonte, PA USA). Trace metal grade 10 M hydrochloric acid and a 0.6%, w/v sodium borohydride solution were pumped at 1 mL min⁻¹ to generate arsine gas. The arsine gas was detected by AAS-F.

RESULTS AND DISCUSSION

Surface area determination. Walker et al. (2006) conducted surface area measurements for arsenopyrite (177–250 μ m) using a NOVA Quantachrome 1000 equipped with nitrogen adsorption. The average specific surface area was reported to be 0.0388 m² g⁻¹. Experimental determinations of specific surface area values using the static BET method were found to be statistically not different from zero with high degree of uncertainty. We infer that arsenopyrite particles used in this study are more soluble than arsenopyrite samples used elsewhere (Walker et al., 2006) because the interfacial energy (γ) is a positive contribution to the total energy according to the equation:

$$\log K_{sp} = \log K_{sp}^{BULK} + \frac{2/3\gamma}{2.3RT} S \quad (1)$$

where K_{sp}' is the conditional solubility product, K_{sp}^{BULK} is the solubility product of the bulk material, S is the surface area per mole, $R = 8.314 \text{ J mol}^{-1} \text{ K}$, and T is the temperature in K (Stumm and Morgan, 1996). Limited predictions using Eqn. (1), however, are to be considered because it assumes that γ is not itself size dependent (Zhang et al., 1999). Also, accurate γ measurements are commonly unavailable, particularly for hydrated surfaces that may be coated with organic ligands.

An exercise to estimate the surface area of the arsenopyrite specimen used in this study was conducted using a geometrical estimation based on particle size and shape. Calculations of the specific surface area (S_{sa}) of 100-149 μm (D) arsenopyrite were conducted assuming a spherical shape for all particles and a density for arsenopyrite (ρ) of 6.09-6.17 g cm^{-3} and according to:

$$S_{sa} = \frac{6}{D\rho} \quad (2)$$

S_{sa} values were found to be in the range 0.0065-0.00985 $\text{m}^2 \text{ g}^{-1}$. For the purpose of comparison, similar estimations using Eqn. (2) for arsenopyrite samples reported to have 0.0388 $\text{m}^2 \text{ g}^{-1}$ as determined by the BET method (Walker et al., 2006) were found to be in the range 0.0038-0.00558 $\text{m}^2 \text{ g}^{-1}$. Experimental and theoretical surface area determinations differ by a factor of 10 or more. Therefore, no attempts to use estimated surface area values to calculate dissolution rates normalized to surface area were conducted. Metal release values are referred to the initial mass of the mineral sample.

SEM-EDX analyses. Experiments to study surface morphology using arsenopyrite crystal samples were conducted. Results are shown in Figure 1 (1(a) through 1(e)).

Arsenopyrite samples were exposed to (I) water only or (II) a 2-mM DFO-B solution. Solid samples were studied after 95 h and 430

h of reaction time. Micrographs of arsenopyrite without treatment show the presence of lead (Figure 1(a)). EDX analyses confirm that lead is in the elemental form (Figure 2). The darker coloration is attributed to a higher Fe content.

Analyses show incrustations of elemental Pb in all arsenopyrite samples, regardless of treatment. Our results contrast with the well-known association of arsenopyrite with sulfide minerals, namely, galena (PbS), pyrrhotite ($Fe_{1-x}S$) ($x = 0$ to 0.2), pyrite (FeS_2) or chalcopyrite ($CuFeS_2$), sphalerite (ZnS), molybdenite (MoS_2), and so on (e.g., Palache et al., 1944). In nature, arsenopyrite is also known to be found in association with gold (Au), bismuth (Bi), and Sn minerals. The authors hypothesize that the presence of incrustations of elemental Pb could be explained in part because highly-reducing conditions prevailed during rock formation.

Figure 1(b) shows arsenopyrite samples exposed to water after 95 h of reaction time. Our results indicate the presence, *albeit* scattered, of small-sized arsenopyrite particles, while dissolution patterns or signs of surface attack are scarcely found. Well-defined borders and growth patterns denote surface crystallinity.

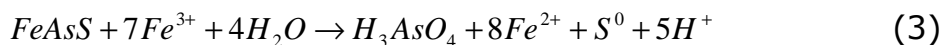
Figure 1(e) show AsSFe exposed to water for 430 h. Well defined growth lines are still evident. This is not the case for arsenopyrite samples exposed to 2 mM DFO-B for 95 h (Figures 1(c) and 1(d)). Micrographs clearly show signatures of mineral dissolution and denote ubiquitous small-sized particles, possibly due to energy lattice disruption and fragmentation. On the other hand, incrustations of elemental Pb show strong attack signatures in the presence of DFO-B (Figure 1(d)). It is worth noting that dissolution effects become more pronounced upon exposure to DFO-B, as compared to water only. Figure 1(d) depicts thin erosion lines throughout the mineral surface and fractures. Figure 1(d) also depicts Pb incrustations with evidence of erosion throughout the mineral surface becomes evident. The more extensive weathering of Pb could

be interpreted to mean faster dissolution kinetics associated with the former than with the latter.

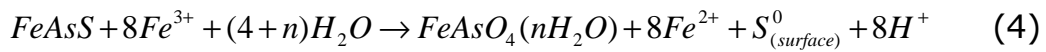
Data listed in Table 1 show elemental analyses of arsenopyrite crystal samples exposed to varying solution compositions at t = 95 and 430 h. As evidenced by S surfaces enrichment with corresponding data for Fe and As release (Figures 3 and 4), the following observations can be drawn:

Samples exposed to 2 mM DFO-B show comparable amounts of structural Fe relative to samples exposed to water only. These observations contrast with solution composition data (Figure 3), and are consistent with mineral dissolution. By contrast, samples exposed to 2 mM DFO-B show enrichment in As relative to those samples exposed to water only, and are consistent with trends in As release (Figure 4). Likely, the mechanisms for Fe and As release are independent of the solution chemical composition, and from each other.

Arsenopyrite samples exposed to 2 mM DFO-B show enrichment in S relative to those samples exposed to water only (Table 1). These findings agree well with reports of elemental sulfur deposition on AsSFe (Steudel, 1996; Cruz et al., 1997; Rohwerder et al., 2003). Voltammetric and XRD studies of the biogenic dissolution of arsenopyrite report that the precipitation of elemental sulfur occurs as a consequence of abiotic and biotic mechanisms (Rohwerder et al., 2003). In the former case, authors attribute elemental sulfur precipitation to Fe^{3+} ions that induce the formation of passive layering according to the reaction:



The precipitation of elemental sulfur can also occur as a consequence of arsenopyrite oxidation in the presence of *Thiobacillus ferrooxidans* according to the reaction:



The formation of elemental sulfur has been explained because the oxidation of aqueous sulfur species in the presence of transition metals including Fe(III) at slightly acidic pH (Steudel, 1996). Metal sulfides such as sphalerite, galena, arsenopyrite, chalcopyrite, and hauerite (ZnS, PbS, FeAsS, CuFeS₂, and MnS₂, respectively) dissolve through both electron extraction by iron(III) ions and proton attack (Rohwerder et al., 2003). In the absence of iron(III) ions, bacteria oxidize free sulfide (H₂S) resulting from the proton attack on the metal sulfide *via* elemental sulfur to sulfuric acid. Such reaction mechanism entails the regeneration of protons previously consumed because metal sulfide dissolution.

Variations of pH. Figure 5 shows the variation of pH in the supernatant solution of arsenopyrite suspensions exposed to water or DFO-B. Our results show the positive variations in pH resulting from long-term reaction of arsenopyrite. This is particularly true in the case of water. Decreases in pH values are observed only within the first 4 h of reaction time. A progressive increase in pH values is recorded within 30 h reaction time, regardless of solution composition. Steady changes in pH values occurred for $t > 30$ h. The more quantitative changes of pH observed in the absence of DFO-B can be explained in part due to DFO-B acid-base equilibria in suspension. At time $t = 0$, DFO-B is mostly present as DFO-B⁺. After 4 h, decreases in [DFO-B⁺] were coupled with increases in [DFO-B], while the pH value approached that of the pKa for the DFO-B⁺/DFO-B acid-base pair, 8.1 (Telford and Raymond, 1996). These observations are consistent with the idea that the DFO-B acid-base pair could be serving as a buffer.

Data plotted in Figure 5 indicate that variations in proton activity did not have an effect in the release of As after reacting

arsenopyrite at $t < 30$ h, regardless of the presence of DFO-B. Furthermore, the amounts of Fe found in suspensions containing DFO-B at $t < 30$ h were found to surpass those found in the presence of water only. The effect of DFO-B on Fe release became evident within the first hours of reaction time. It follows that ligand-promoted dissolution dominates over proton-promoted dissolution in spite of the fact that the recorded pH values were found to be lowest at $t < 30$ h.

It is worth noting that variations in pH following arsenopyrite dissolution in the presence of DFO-B or water only contrast with a report (Rohwerder et al., 2003) on increases in proton activity following biogenic dissolution of arsenopyrite as described by Eqns (3) and (4), and are inconsistent with independent mineral dissolution mechanisms.

Release of Fe, As, and Pb. Our results show that following exposure of arsenopyrite ($100\text{-}149 \mu\text{m}$, 1 g L^{-1}) to water at $\text{pH} = 5$ after 5 days total soluble As can be as high as 0.15 ppm. Thus, arsenopyrite specimens were prewashed prior to use. Figure 3 shows the amounts of dissolved Fe following the reaction of arsenopyrite with water or DFO-B containing solutions at $\text{pH} 5$. In the presence of water, variations in Fe are negligible even after 110 h of reaction time. In the presence of DFO-B, however, releases of Fe increases with time. These results coincide with observed decreases in % Fe in arsenopyrite samples exposed to similar reaction conditions (Table 1). This is particularly the case at longer reaction times.

Figure 4 shows the effect of $200 \mu\text{M}$ DFO-B on the dissolution behavior of mineral As. At reaction times < 40 h, the presence of DFO-B on mineral dissolution was found to have a negligible effect. The effect of DFO-B on mineral dissolution became evident at longer reaction times. After 110 h, the dissolution of As in the presence of water only and DFO-B corresponded to 0.151 ± 0.003 and 0.270 ± 0.009 ppm of As, respectively.

Figure 6 summarizes data pertinent to the extent of As, Fe, and Pb release with time. At reaction times surpassing 110 h, dissolved Fe and As values were found to be as high as 0.328 ± 0.006 ppm and 0.270 ± 0.009 ppm, respectively. Our results can be explained because a non-conservative mineral dissolution pathway. In the presence of DFO-B, the concentration of soluble Pb was found to be ca. 0.144 ± 0.005 ppm. By contrast, in the presence of water only, the concentration of soluble Pb was found below the analytical detection limits (< 0.05 ppm).

Elemental analyses. Arsenopyrite samples were digested in acid (25 g L^{-1} ; 0.5 g arsenopyrite in 20 mL HNO_3 70%) for 5 days. Brownish vapors were liberated and a yellowish precipitate formed within the first hours of reaction time. These results agree well with reports of releases of sulfur oxides and the formation of elemental sulfur following enzymatic pathways for arsenopyrite dissolution (Rohwerder et al., 2003). Notably, data trends for S sample enrichment parallel that for Fe (Table 1), which could be an indication that the bond energy of Fe-S subunits limits Fe release.

Figure 7 shows the dissolution behavior of Fe, As, and Pb. Y-axis units, % dissolved, correspond to the concentrations of As, Fe, and Pb divided by the total concentrations of As, Fe, and Pb, respectively, $\times 100$. Total concentrations of As, Fe, and Pb were determined by acid digestion. Chemical analyses following acid digestion of arsenopyrite samples (25 g L^{-1}) in nitric acid 70% showed total soluble As, Fe, and Pb to be ca. 13950, 13417, and 434 ppm, respectively. Therefore, total concentrations of Pb, As, and Fe following exposure of 1 g L^{-1} arsenopyrite either DFO-B or water only were not expected to surpass 17.4 ppm, 558 ppm, and 537 ppm, respectively. Maximum detected concentrations (after 110 h reaction time) of Pb, As, and Fe were ≤ 0.15 ppm (ca. 1% total Pb), ≤ 0.27 ppm (0.05% of the total As), and ca. 0.328 ppm (0.06% total Fe), respectively. It can be seen that while on a molar basis the

effectiveness of DFO-B for releasing Fe and As is comparable, the effectiveness of DFO-B for releasing Pb is ten times that for releasing either Fe or As. These kinetic observations for the release of Pb cannot be accounted for by thermodynamic considerations for metal complexation by DFO-B alone (Herlnem et al. 1999).

As speciation. Listed in Table 2 are data pertinent to the speciation of As after reacting arsenopyrite (100-149 μ m) with (a) water (closed circles) and (b) 200 μ M DFO-B (closed squares) at pH₀ 5. In both scenarios, there are variations in the As(III)/As(V) ratio with time. At reaction times < 30 h, concentrations of As(V) were found to be as high as 50-70%, regardless of the presence of DFO-B. At longer reaction times, 30 < t < 120 h, however, As undergoes reduction from As(V) to As(III). As(III) becomes the predominant As species in solution (Table 2) with no concomitant variations in pH (Figure 5). It follows that the reduction of As(III) cannot be accounted for by evidence of sulfur oxidation alone (Table 1). The lack of variation in proton activity following fluctuations in As speciation (arguably due to sulfur oxidation) serves as an indication that mechanisms other than Eqns (3) or (4) prevail in suspension.

Arsenic speciation and dissolved oxygen concentration. Shown in Figure 8 are data trends pertinent to dissolved oxygen concentrations in arsenopyrite suspensions in the presence of DFO-B or water only. The dissolved oxygen concentration vary with solution composition:

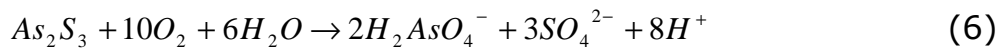
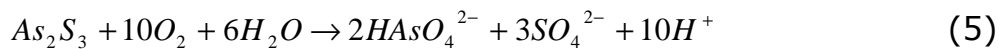
In the presence of water and a) at t = 3 h of reaction time there are no decreases in dissolved oxygen concentration, [O₂] and there is evidence to show As(V) accumulation; then, for the case of t = 30 h, there is little variation of [O₂] coupled with increasing accumulation of As(V); for the case of t = 60 h, our data show decreases in [O₂] coupled with the accumulation of As(III) and the depletion of [As(V)], a signature of suboxic conditions. At longer reaction times, t = 110 h, [O₂] increases albeit slightly while As(III)

accumulates steadily. Taken together, these observations indicate that dissolved molecular oxygen does not serve as ultimate electron acceptor towards arsenic in an exclusive manner.

The presence of DFO-B in arsenopyrite suspensions affects the speciation of As and dissolved oxygen concentration. Our results show that at short reaction times, $t = 3$ h, there is a sharp depletion of $[O_2]$ coupled with the accumulation of As(V). Yet, at longer reaction times, $t = 30$ h, $[O_2]$ increases while the concentrations of As(III) and As(V) remain invariant. These results serve as an indication that $[O_2]$ participates in existing reaction mechanisms in suspension in addition to those controlling As redox cycling. This proposal is further confirmed because at $t = 60$ h, our data show no variations in $[O_2]$ coupled with the quantitative accumulation of As(III) in solution. It is worth a pause to note that the lack of variation of Fe(III) as affected by $[O_2]$ at $0 < t < 110$ h. Thus, we discard the notion that iron redox cycling may be controlling speciation of As in suspension. At the same time, fluctuations in the As(III)/As(V) ratio occur at earlier reaction times, $t < 60$ h, as evidenced by the lack of variation in $[O_2]$, [As(III)], and [As(V)] at $t = 120$ h. We note that stabilizing mechanisms for As(III) ought to prevail in suspension for them to outcompete oxidation of As(III) to As(V) by O_2 .

Thus far, data presented herein provides evidence to show that DFO-B influences proton exchange reactions which could exert an effect in sulphur speciation [Eqs. (3) and (4)]. EDX analyses conducted on arsenopyrite surfaces (Table 1) show higher accumulation of sulphur in samples exposed to DFO-B. These results coincide with observed lower contents of O_2 in arsenopyrite suspensions containing DFO-B (Figure 8). As discussed above, there is a lack of correlation between As speciation and dissolved oxygen concentration prevails. In this scenario, sulphur speciation becomes pivotal for As redox cycling.

Like orpiment and amorphous As_2S_3 , arsenopyrite is thought to undergo oxidative dissolution with the concomitant oxidation of sulphur by dissolved oxygen (Lengke and Tempel, 2002). It has been proposed that like for pyrite oxidative dissolution, sulphur may be predominantly in the form of polythionates following mineral dissolution at circumneutral pH (Goldhaber, 1983; McKibben and Barnes, 1986; Moses et al., 1987). The lifetime of polythionates has been reported as (Lengke and Temple, 2002) short arguably due to their quick removal from near the pyrite surface, which acts as catalysts for their oxidation to sulfate. Reportedly, Eqn. (5) and (6) proceeds in an incomplete manner and cannot account for by experimental observations (Lengke and Temple, 2002):



A related report of PHREEQC calculations (Parkhurst, 1995) indicate that As(III) exists predominantly as H_3AsO_3 [Eqn. (7)] and As(V) as HAsO_4^{2-} [Eqs. (5) and (6)]. Yet, steady-state dissolution experiments on orpiment oxidation at pH 6.8 to 8.2 show that the ratio of As(III)/As(V) is 1.1 to 2.2, regardless of the total As concentration (Lengke and Temple, 2002). In that study, the rate of orpiment oxidation was found to depend on the concentration of dissolved oxygen content within the range of oxygen concentration studied (6.4 to 17.4 ppm O_2 ; Lengke and Temple, 2002). In this paper, it becomes clear that As(III)/As(V) ratio values following arsenopyrite dissolution (Table 2) can be significantly higher ($t \leq 110$ h) than reported As(III)/As(III) values for orpiment (Lengke and Temple, 2002). Furthermore, our experiments on arsenopyrite dissolution show that there is a lack of correlation between As redox

cycling (Table 2) and oxygen concentrations (Figure 8). Therefore, conjectures on common dissolution mechanisms pathways cannot be withdrawn. Rather, discrepancies between experimental results are interpreted to mean that parallel dissolution pathways of minerals bearing As and S take place. We do not discard the possibility that polythionates may participate in As redox cycling during arsenopyrite dissolution.

Interaction between DFO-B and arsenopyrite surfaces. The effect of reaction time on the adsorption behavior of DFO-B on the surface of arsenopyrite at pH₀ 5 was studied. Our results show small variations of DFO-B concentration after 110 h reaction time and, as a consequence, determinations of DFO-B surface excess values were found to be within error (not shown). These observations suggest that the kinetics for ligand-surface complexation is fast, while that of desorption is slower. A lack of correlation between pH variations at reaction times $t \leq 24$ h (Figure 5) with DFO-B adsorption behavior further indicates that variations in pH have an effect *albeit* small on the amount of free DFO-B in solution (not associated with the mineral surface).

The poor surface affinity of DFO-B is explained because the small number of adsorption sites (e.g., $a_s \sim 0.0388\text{ m}^2\text{ g}^{-1}$; Walker et al., 2006). In addition, plausible steric hindrance encountered by DFO-B while attempting to complex an Fe(III) center in the mineral may still play a role. Cocozza et al. (2002) have hypothesized that both hydrophobic and stereochemical effects limit the siderophore to bind with only one of its three hydroxamate groups for complexing Fe(III) centers.

Release of structural Pb. To further understand the influence of the presence of Pb in the structure of arsenopyrite on mineral dissolution, experiments were conducted to study the dissolution behavior of galena (PbS) in the presence of 200 μM DFO-B at pH₀ = 5. Data pertinent to Pb release and pH variations with time are shown

in Figures 9 and 10. Like for arsenopyrite, the presence of DFO-B influences the magnitude of gradients in proton concentration. By comparison, for the case of arsenopyrite, there is a shallower net gradient in proton concentrations imposed in the presence of DFO-B compared to that of water only (Figures 5 and 10). For the case of galena in the presence of water, variations in proton activity take place at long reaction times ($t > 80$ h). These results contrast data pertinent to arsenopyrite suspensions in water showing variations in pH at short reaction times, a signature of proton exchange equilibria. In the presence of DFO-B, suspensions containing arsenopyrite or galena, variations in pH in suspensions are still shallow (Figure 10). These results agree well with the hypothesis that DFO-B acid-base pair can serve as a buffer in suspension. Unlike the dissolution behavior of arsenopyrite (Figures 3 through 5), the dissolution behavior of galena shows coupled increases in pH with decreases in metal solubility at $t > 80$ h (Figures 9 and 10). The consumption of protons, increase in $\{\text{OH}^-\}$ activity, in suspension holds true, regardless of the presence of DFO-B.

Recent studies (De Giudici et al., 2005; 2007) have reported the dissolution of cleaved (001) galena at $1.2 < \text{pH} < 5.8$ under oxic conditions. As determined by fluid-cell micro-Raman Spectroscopy (μRS), following dissolution a layer of several tens to hundreds of nanometers composed of Pb oxides, sulfates, and sulfur metastable species forms at the galena surface (De Giudici et al., 2007). Reportedly, galena dissolution rates decrease with pH and reaction time. Our results (Figures 9 and 10) display similar trends in reactivity after the reaction between galena and DFO-B at $\text{pH}_0 = 5$. De Giudici et al. (2007) have attributed the formation of Pb oxides to sulfur partial oxidation. Arguably sulfur oxidation occurs at the interface due to reaction with dissolved O_2 with S atoms at the galena surface, or in the immediate vicinity. Subsequently, oxygen combines with Pb ions to form Pb oxide at the interface. We do not discard the

notion that small-sized lead oxides form upon dissolution of Pb (Figure (1b)) and dissolving sulphur.

Exposure of different sources of Pb(II) bearing different initial amounts of structural Pb, namely, arsenopyrite and galena, to 200 μM DFO-B led to the release of *ca.* 1% and 5% total soluble Pb (as determined by acid digestion), respectively. In the former case, DFO-B is present in molar excess relative to Pb. By comparing the amount of Pb released in both scenarios, it becomes clear that mineral Pb, structural or adsorbed, limits mineral dissolution.

Oxidative dissolution mechanisms conveying sulfur oxidation bring about the production of $\{\text{H}^+\}$ (e.g., Nordstrom and Archer, 2003). However, dissolution data trends for arsenopyrite and galena indicate the consumption of $\{\text{H}^+\}$ (Figures 5 and 10). Our results show that the presence of DFO-B affects both variations in proton activity with time and the release of Pb. Thus, it is expected that, aside of the formation of Pb oxides (De Giudici et al., 2007), other Pb species dependent on $\{\text{H}^+\}$ and $\{\text{OH}^-\}$ may be forming in suspension. In this light, the authors note speciation considerations reported elsewhere (see Table 3 after Kraemer et al., 2002) and the plausible formation of stable surface hydroxyl complexes of the form $\text{Pb}_4(\text{OH})_4^{4+}$ ($\text{pH}_{50}=5.8$) and $\text{Pb}_6(\text{OH})_8^{4+}$ for pH values 5.8 or above (Baes and Mesmer, 1976).

CONCLUSIONS

In this manuscript the authors have reported the dissolution of arsenopyrite and galena(1 g L^{-1}) in the presence of a siderophore ligand (desferrioxamine-B, DFO-B) at $\text{pH}_0 = 5$ for 140 h.

Detected concentrations of soluble Fe, As, and Pb in suspensions containing water only were found to be *ca.* 0.09 ± 0.004 , 0.15 ± 0.003 , and 0.01 ± 0.01 ppm, correspondingly. In contrast,

concentrations of soluble Fe, As, and Pb in suspensions containing DFO-B were found to be 0.4 ± 0.006 , 0.27 ± 0.009 , and 0.14 ± 0.005 ppm, respectively. Notably, the effectiveness of DFO-B for releasing Pb was almost ten times higher than that for releasing Fe. Our results show that the dissolution of arsenopyrite leads to precipitation of elemental sulfur, and is consistent with a non-enzymatic mineral dissolution pathway. Speciation analyses for As indicate variability in the As(III)/As(V) ratio with time, regardless of the presence of DFO-B or water only. At reaction times $t < 30$ h, As(V) concentrations were found to be 50-70%. This is true regardless of the presence of DFO-B. Hence, redox transformations of As are not accounted for by ligand-mediated mechanisms. This paper provides evidence to show that As speciation, and thus toxicity, following biogenic arsenopyrite dissolution may occur due to non-enzymatic pathways.

Our findings agree well with reports of elemental sulfur deposition on AsSFe (Steudel, 1996; Cruz et al., 1997; Rohwerder et al., 2003) as a consequence of abiotic [Eqn. (3)] and biotic mechanisms [Eqn. (4)]. On a molar basis, iron release values following weathering of arsenopyrite in the presence of siderophore ligands were found to be much lower than values reported as a consequence of arsenopyrite oxidation in the presence of *Thiobacillus ferrooxidans*

(Monroy-Fernandez et al., 1995). Incubations of $32\text{-}53 \mu\text{m}$ arsenopyrite (20 g L^{-1} suspension) with *Thiobacillus ferrooxidans* at pH 1.8 under oxic conditions reportedly brings about Fe releases of approximately 100 ppm after 4 d, increasing to 1000 ppm after 30 d (Monroy-Fernandez et al., 1995). Experiments were also conducted to study the dissolution behavior of galena (PbS) (1 g L^{-1}) in the presence of $200 \mu\text{M}$ DFO-B at $\text{pH}_0 5$. The solubility of galena decreases with pH and time. The consumption of $\{\text{H}^+\}$ during the dissolution of galena was explained through the possible formation of

stable surface hydroxyl complexes of the form $\text{Pb}_4(\text{OH})_4^{4+}$ ($\text{pH}_{50}=5.8$) and $\text{Pb}_6(\text{OH})_8^{4+}$ for pH values 5.8 or above.

Acknowledgments

Hilda Cornejo-Garrido gratefully acknowledges the support of an undergraduate fellowship from The National Autonomous University of Mexico [DGAPA-UNAM, PAPITT (Grant No. IN116007-2)]; Javiera Cervini-Silva thanks the support of the Mexican Academy of Sciences (Academia Mexicana de Ciencias) and The United States-Mexico Foundation for Science (Fundación México-Estados Unidos para la Ciencia) through the 2006-Young Researcher Summer Program Fellowship (AMC-FUMEC). The authors are most grateful to Kent Ross (University of California Berkeley) for providing mineral samples; to Elizabeth Chávira (Instituto de Investigación en Materiales, UNAM), Sergey Sedov (Instituto de Geología, UNAM), and Gretchen Lapidus Lavine (Universidad Autónoma Metropolitana, Itzapa) for technical assistance. This research was in part supported by The National Autonomous University of Mexico [DGAPA-UNAM, PAPITT (Grant No. IN116007-2)], CONACYT [SEP-CONACYT Ciencia Básica 2006, Grant no. 61670], and the UC MEXUS Program. The original form of this manuscript was improved significantly thanks to comments by one anonymous reviewer, Dave Craw (U. Otago, New Zealand), D. Kirk Nordstrom (U.S. Geological Survey, Boulder, CO) and Rebecca Sutton (Environmental Working Group, Oakland, CA).

TABLES

Table 1. EDX Analyses of Arsenopyrite Crystals Exposed to Aqueous Solutions of 200 mM DFO-B at pH₀ 5.

	Fe	As	S		Fe	As	S
No treatment							
	31.8 ± 2.8	33.1 ± 2.2	35.1 ± 0.7				
Water							
200 mM DFO-B							
time (h)							
95	34.6 ± 1.9	32.9 ± 1.3	32.5 ± 0.5	32.8 ± 0.7	31.7 ± 1.4	35.5 ± 2.1	
432	31.9 ± 1.9	34.9 ± 0.5	33.2 ± 1.4	30.6 ± 0.9	33.7 ± 1.1	35.7 ± 6	

Table 2. Speciation of As after the Reaction between Arsenopyrite and 200 µM DFO-B at pH₀ 5.

Time (h)	Water			200 µM DFO-B		
	As(III)	As(V)	As total	As(III)	As(V)	As total
0	98.4 ± 0.4	1.64 ± 0.4	0.04 ± 0.01	99.4 ± 0.3	0.6 ± 0.3	0.03
4	52.4 ± 8.5	47.5 ± 4.5	0.1 ± 0.01	35.9 ± 11.5	64.1 ± 11.5	0.15 ± 0.07
27	28.9 ± 7.4	71.1 ± 7.4	0.5 ± 0.04	43.2 ± 10.4	56.8 ± 10.4	0.6 ± 0.05
58	78.1 ± 4.2	21.9 ± 4.2	0.5 ± 0.07	94.2 ± 4.2	5.8 ± 4.25	0.65 ± 0.07
110	96 ± 7.6	4.01 ± 0.60	0.5 ± 0.05	81.6 ± 7.6	18.4 ± 7.6	1.10 ± 0.09

Table 3. Conditional Formation Constants (Kc) used in Model Calculations PHREEQC (Parkhurst, 1995) for the System Lead and DFO-B in Water.

	Log Kc		Log
			Kc
$DFO^{3-} + H^+ \leftrightarrow HDFO^{2-}$	10.46	$CO_3^{2-} + OH^- + Pb^{2+} \leftrightarrow PbOHC$	10.70
$HDFO^{2-} + H^+ \leftrightarrow H_2DFO^-$	9.35	$OH^- + Pb^{2+} \leftrightarrow PbOH^-$	6.58
$H_2DFO^- + H^+ \leftrightarrow H_3DFO$	8.90	$2OH^- + Pb^{2+} \leftrightarrow PbOH_2(aq)$	11.18
$H_3DFO + H^+ \leftrightarrow H_4DFO^+$	8.38	$3OH^- + Pb^{2+} \leftrightarrow PbOH_3^-$	14.23
$HDFO^{2-} + Pb^{2+} \leftrightarrow PbHDFO$	9.48	$OH^- + 2Pb^{2+} \leftrightarrow Pb_2OH^{3+}$	7.61
$H_2DFO^- + Pb^{2+} \leftrightarrow PbH_2DFO^+$	8.99	$4OH^- + 3Pb^{2+} \leftrightarrow Pb_3(OH)_4^{2+}$	32.66
$H_3DFO + Pb^{2+} \leftrightarrow PbH_3DFO^{2+}$	5.92	$4OH^- + 4Pb^{2+} \leftrightarrow Pb_4(OH)_4^{4+}$	36.20
$HDFO^{2-} + 2Pb^{2+} \leftrightarrow Pb_2HDFO^{2+}$	15.77	$8OH^- + 6Pb^{2+} \leftrightarrow Pb_6(OH)_8^{4+}$	69.16
$CO_3^{2-} + Pb^{2+} \leftrightarrow PbCO_3(aq)$	4.56	$CO_3^{2-} + H^+ \leftrightarrow HCO_3^-$	10.46
$2CO_3^{2-} + Pb^{2+} \leftrightarrow Pb(CO_3)_2^{2+}$	8.02	$HCO_3^- + H^+ \leftrightarrow H_2CO_3$	6.402
$CO_3^{2-} + Pb^{2+} \leftrightarrow PbCO_3(s, cerrusite)$	-13.49		

All Kc values are corrected to I = 0.01 M. Data as reported in

Kraemer et al. (1999), where Kc values were taken from Martell et al. (1995) and Hernlem et al. (1995).

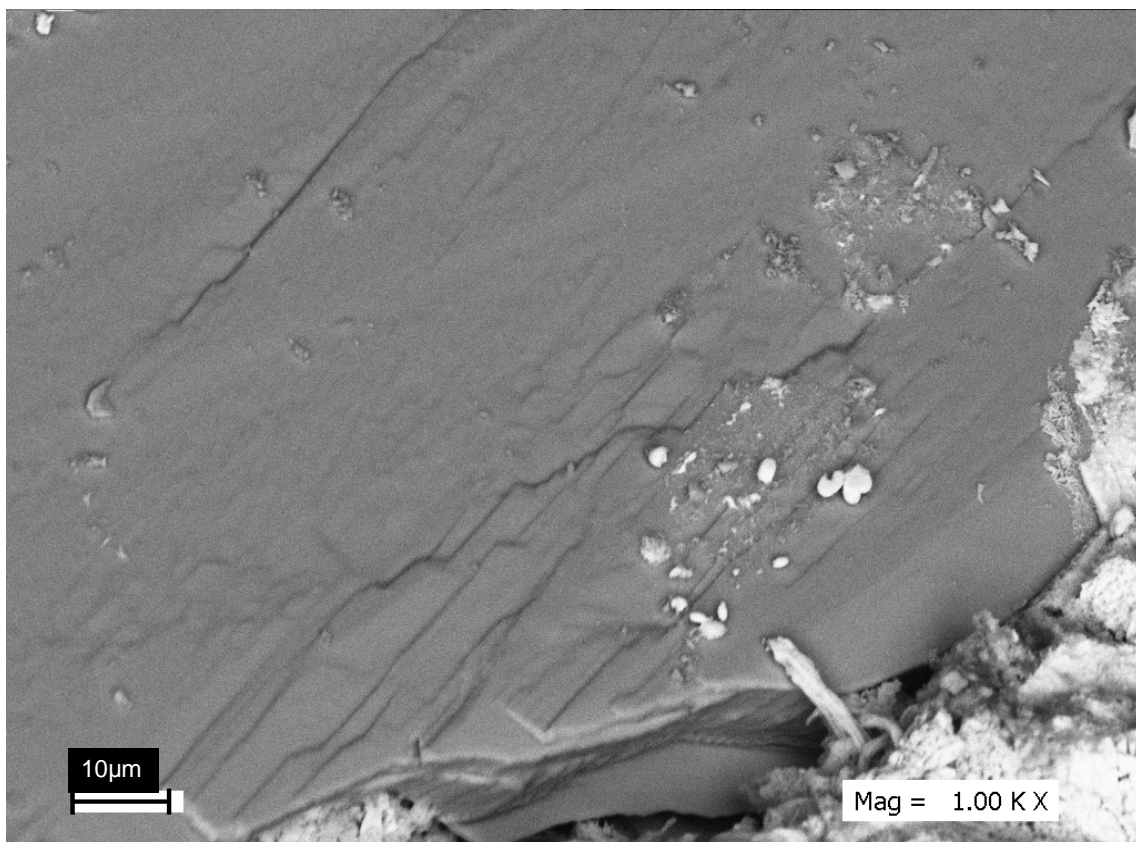


Figure 1. Scanning Electron Micrographs of arsenopyrite cristals.
Figure 1(a) Shows FeAsS before treatment

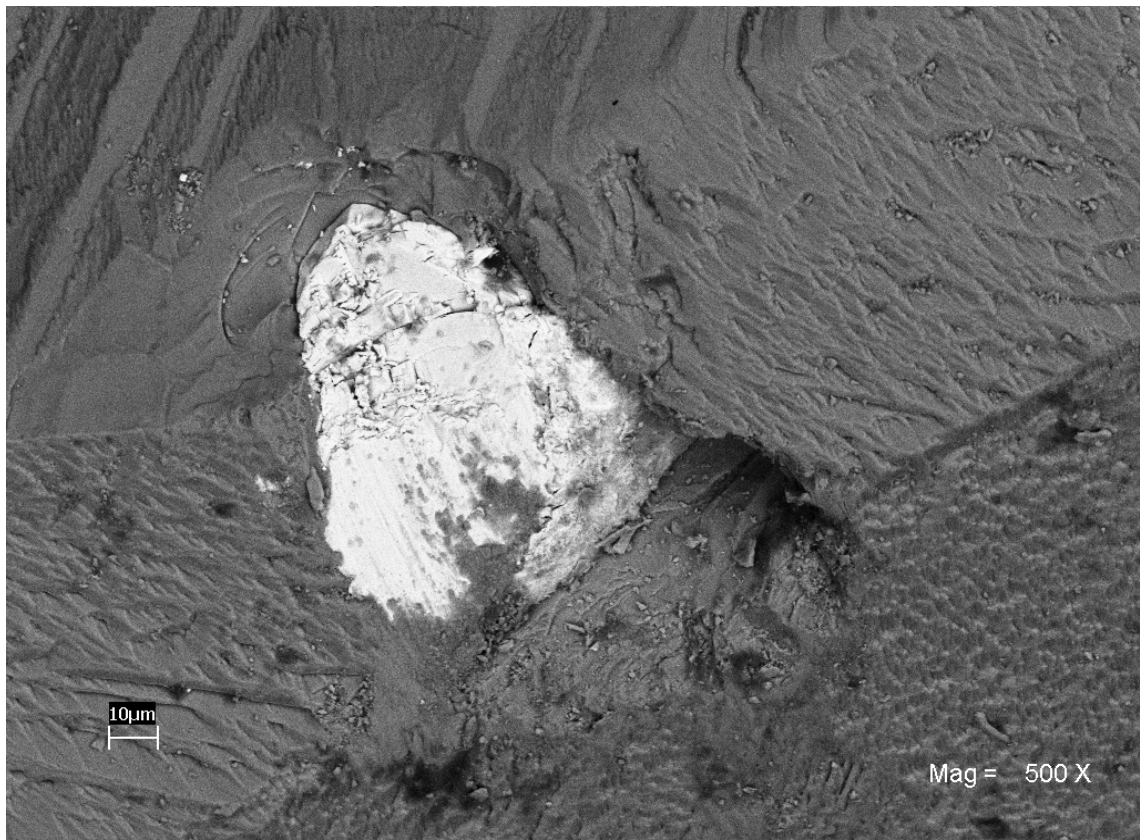


Figure 1(b). Arsenopyrite crystals after 95 h exposure to water at pH = 5.

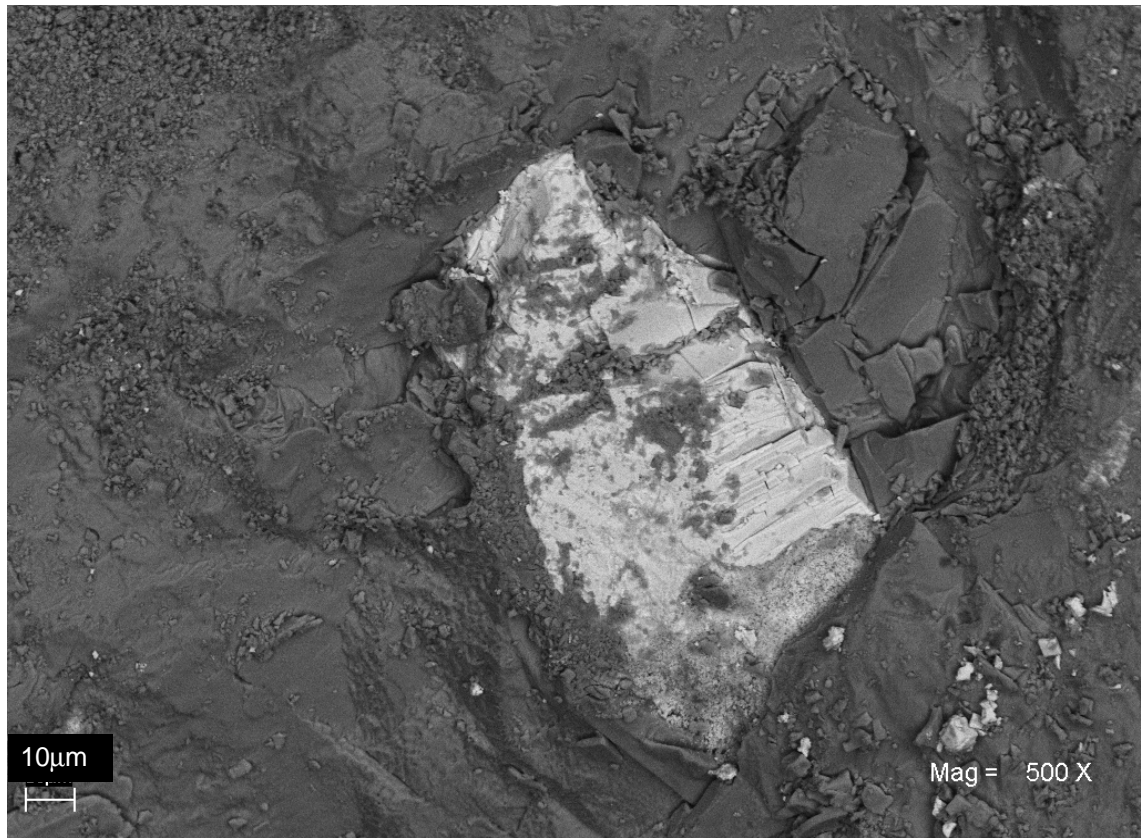


Figure 1(c). Show arsenopyrite crystals after 95 h exposure to 2 mM DFO-B at pH = 5.

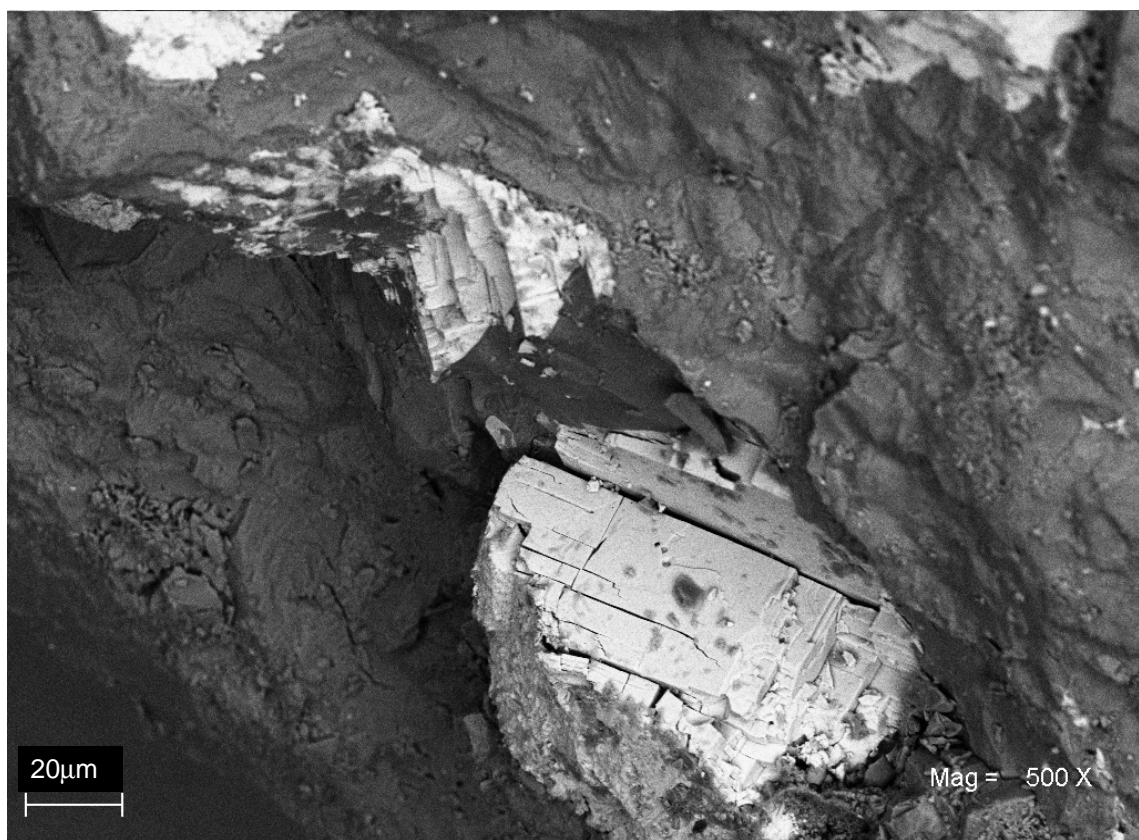


Figure 1(d). Show arsenopyrite crystals after 430 h exposure to 2 mM DFO-B at pH = 5.

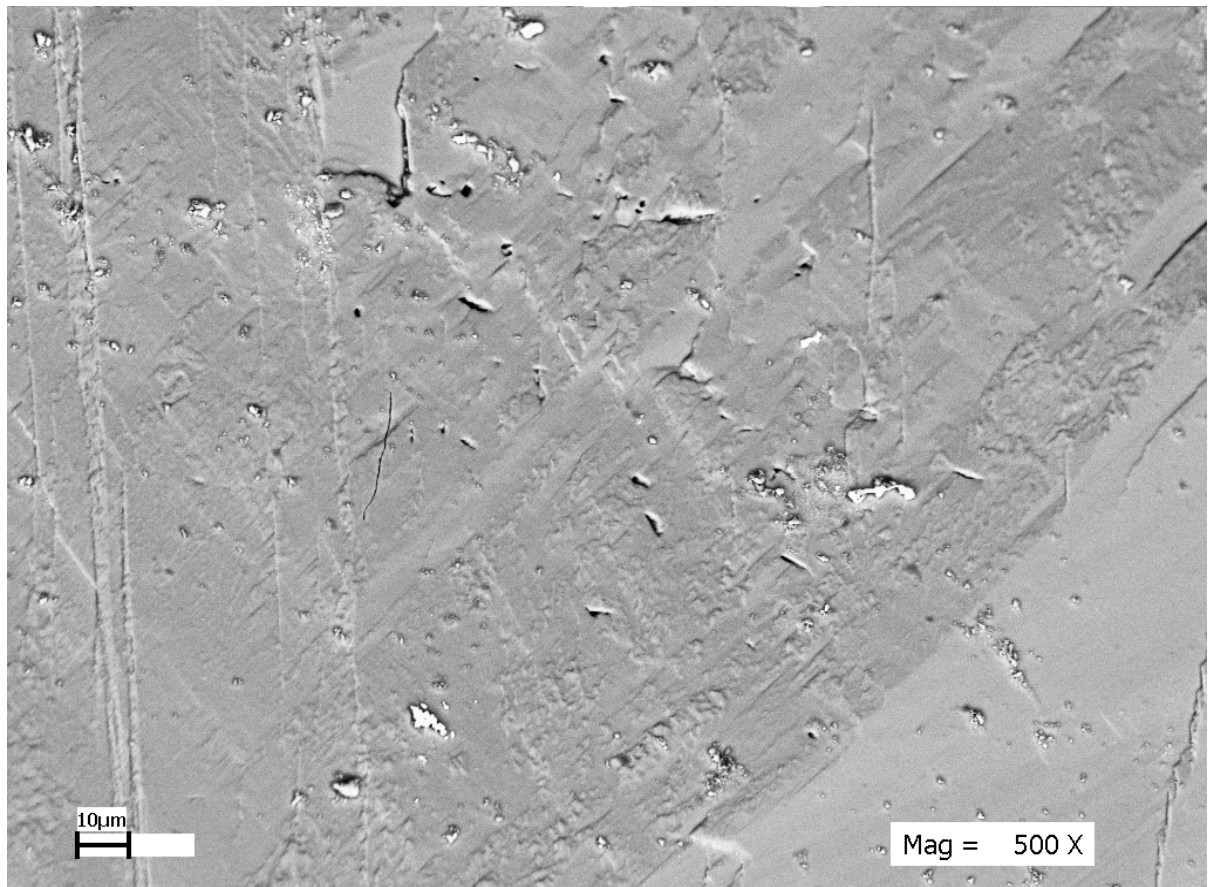


Figure 1(e). Arsenopyrite crystals after 430 h exposure to water.

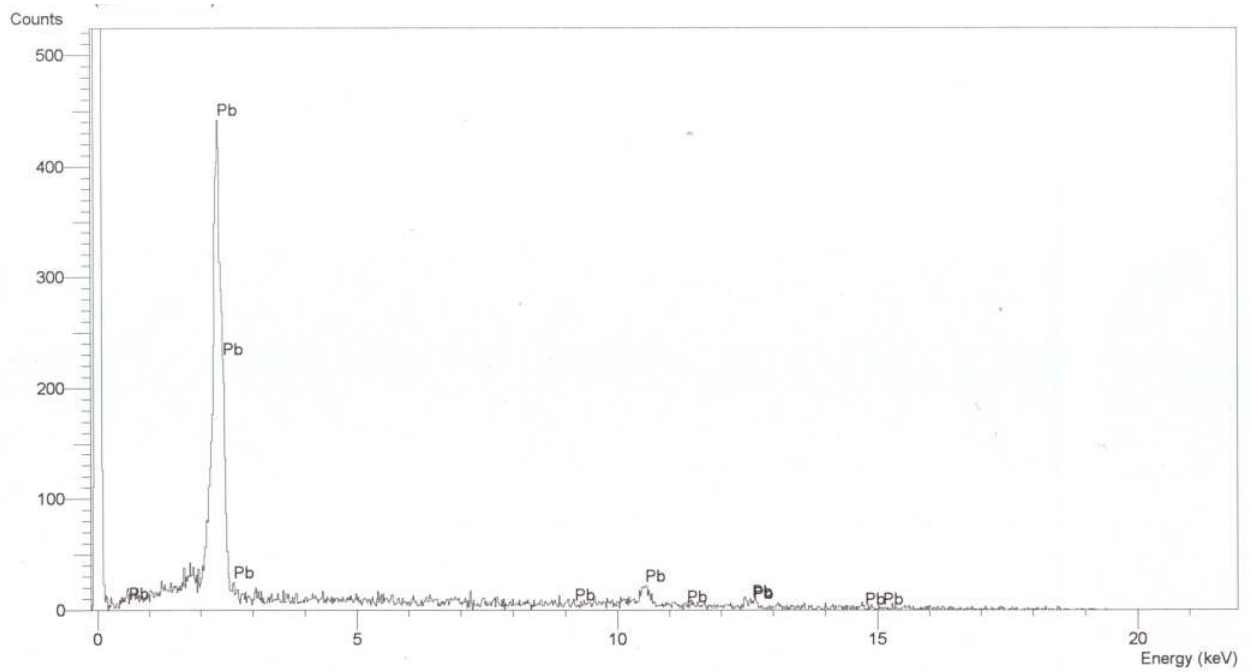


Figure 2. EDX Analysis for arsenopyrite surfaces and the presence of elemental Pb.

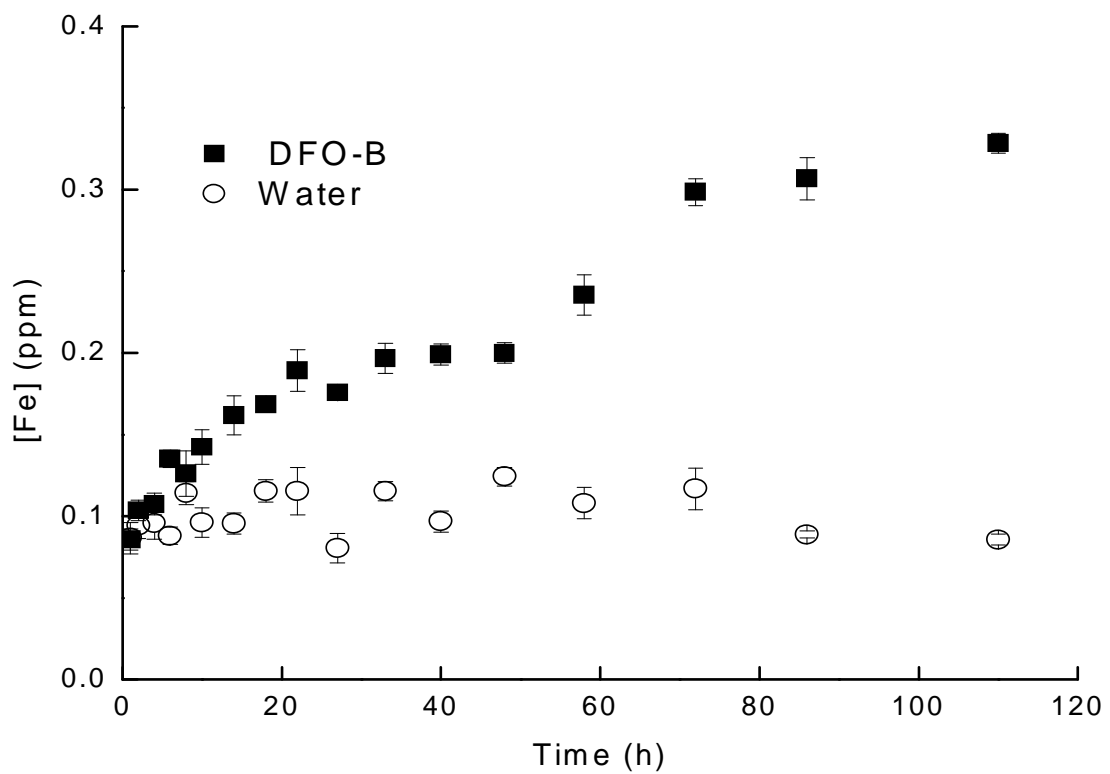


Figure 3. Release of Fe after reacting arsenopyrite (0.149-0.1 mm) with (a) water (open circles) and (b) 200 μ M DFO-B (closed squares) at pH0 = 5.

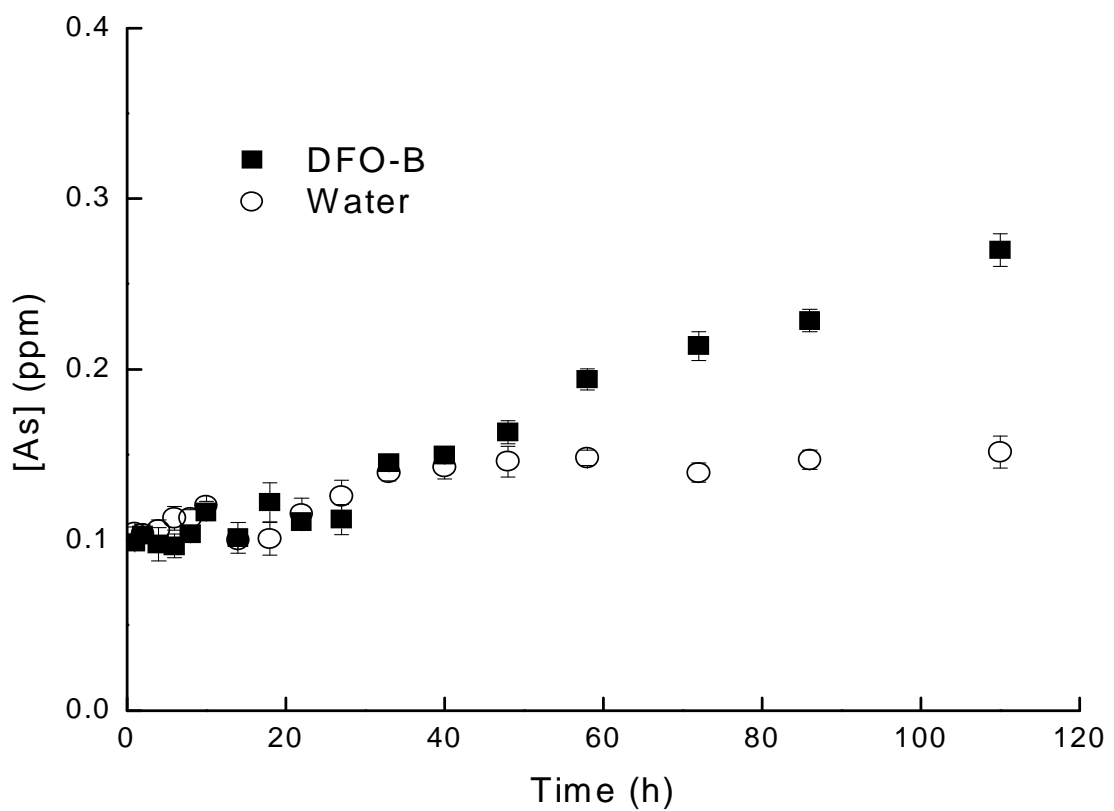


Figure 4. Release of As after reacting arsenopyrite (0.149-0.1 mm) with (a) water (open circles) and (b) 200 μ M DFO-B (closed squares) at pH₀ = 5.

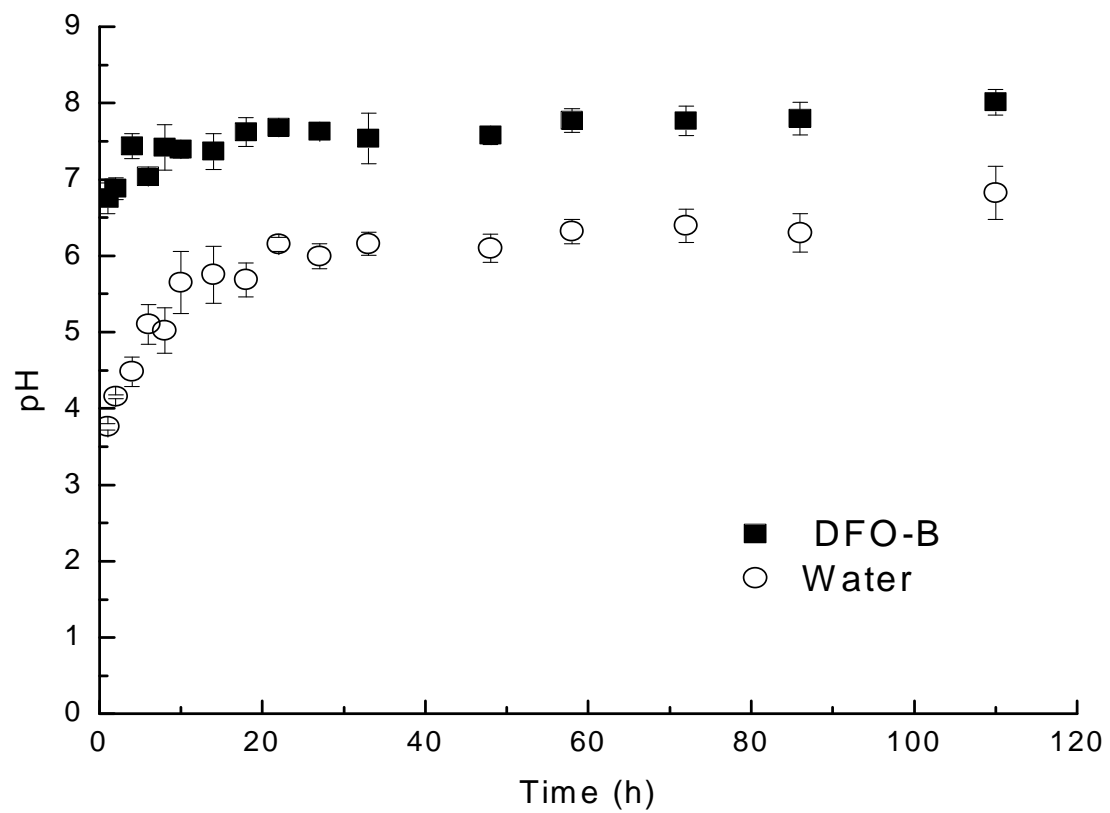


Figure 5. Variations of pH during the reaction between 1 g L⁻¹ arsenopyrite and 200 μM DFO-B.

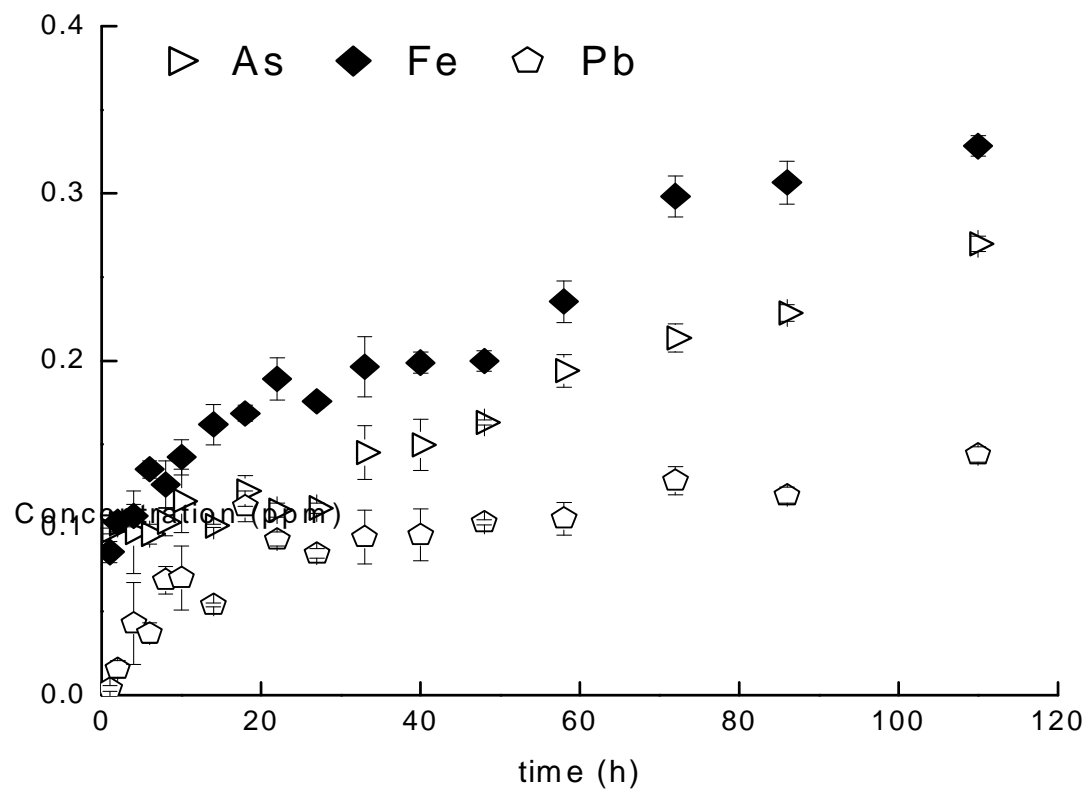


Figure 6. Comparison between the release of As (open triangles), Fe (closed rhomboids), and Pb (open pentagons) after reacting arsenopyrite (0.149 - 0.1 mm) with 200 μM DFO-B at $\text{pH}0 = 5$.

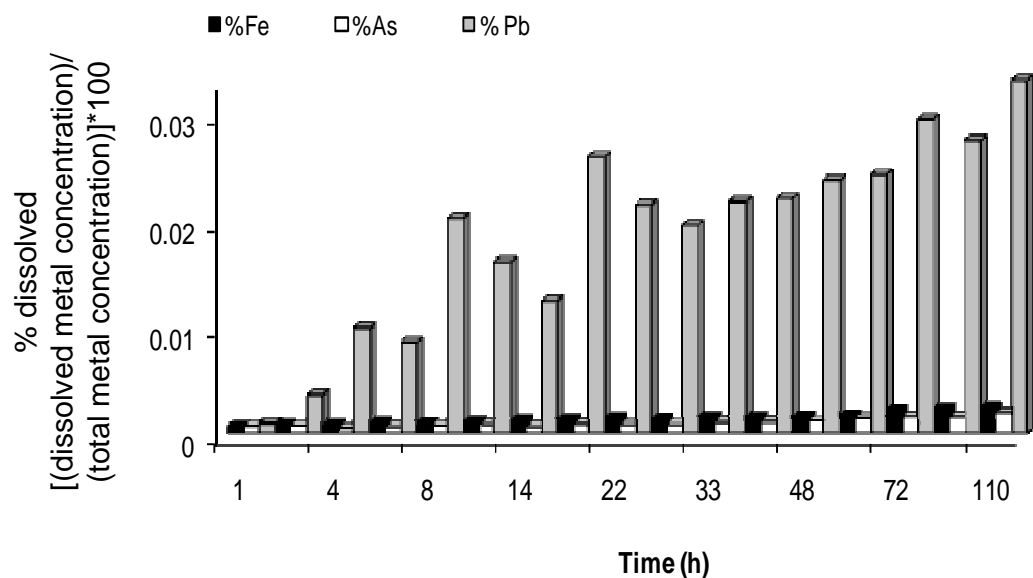


Figure 7. Molar comparison between the release of As, Fe, and Pb after reacting arsenopyrite (0.149 - 0.1 mm) with 200 μM DFO-B at pH0= 5. The y-axis units, % dissolved, correspond to the concentrations of As, Fe, and Pb divided by the total concentrations of As, Fe, and Pb, respectively, $\times 100$. Total concentrations of As, Fe, and Pb were determined by acid digestion.

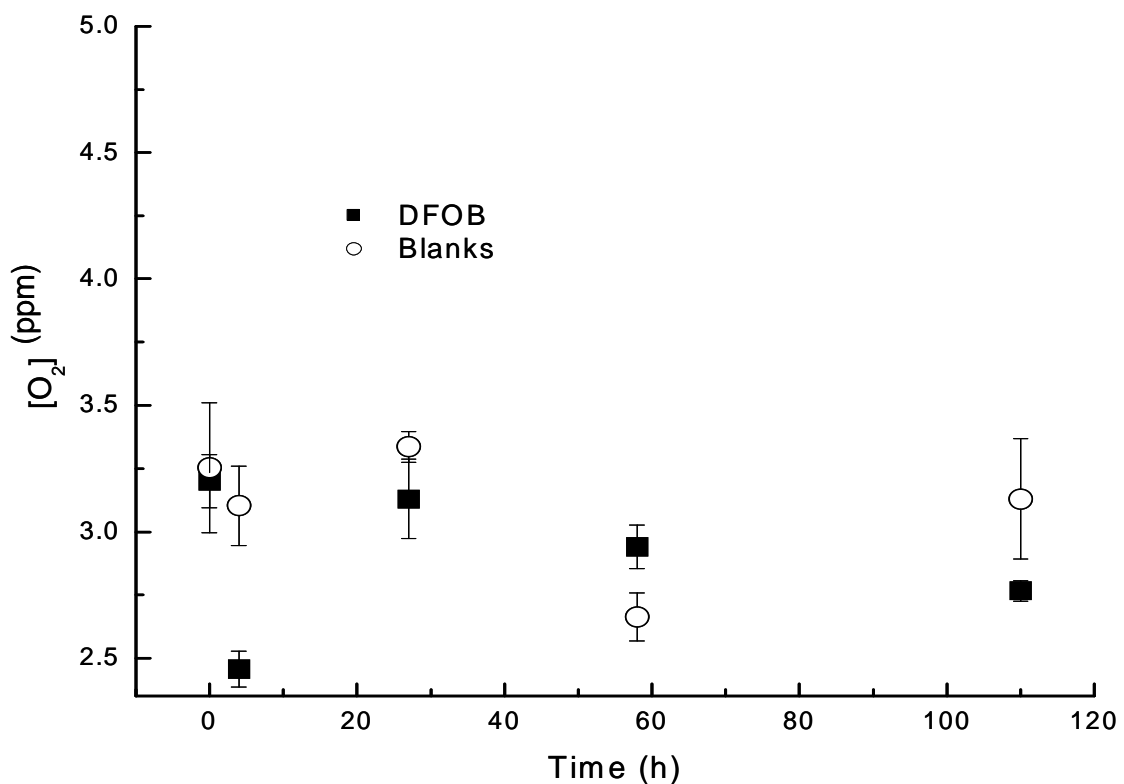


Figure 8. Dissolved oxygen concentration profiles in arsenopyrite suspensions in the presence of (a) water (open circles) and (b) 200 μ M DFO-B (closed squares) pH₀ = 5. The units of dissolved oxygen concentration are ppm.

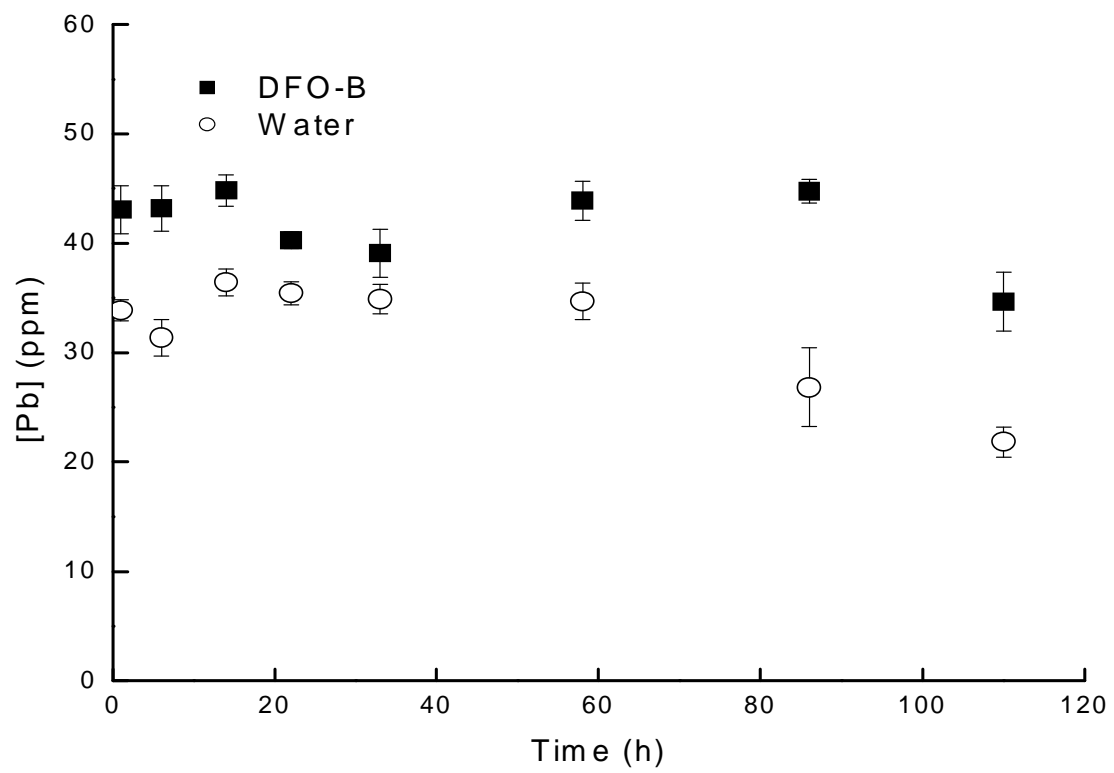


Figure 9. Release of Pb after reacting galena (0.149-0.1 mm) with (a) water (open circles) and (b) 200 μ M DFO-B (closed squares) at pH 0.5.

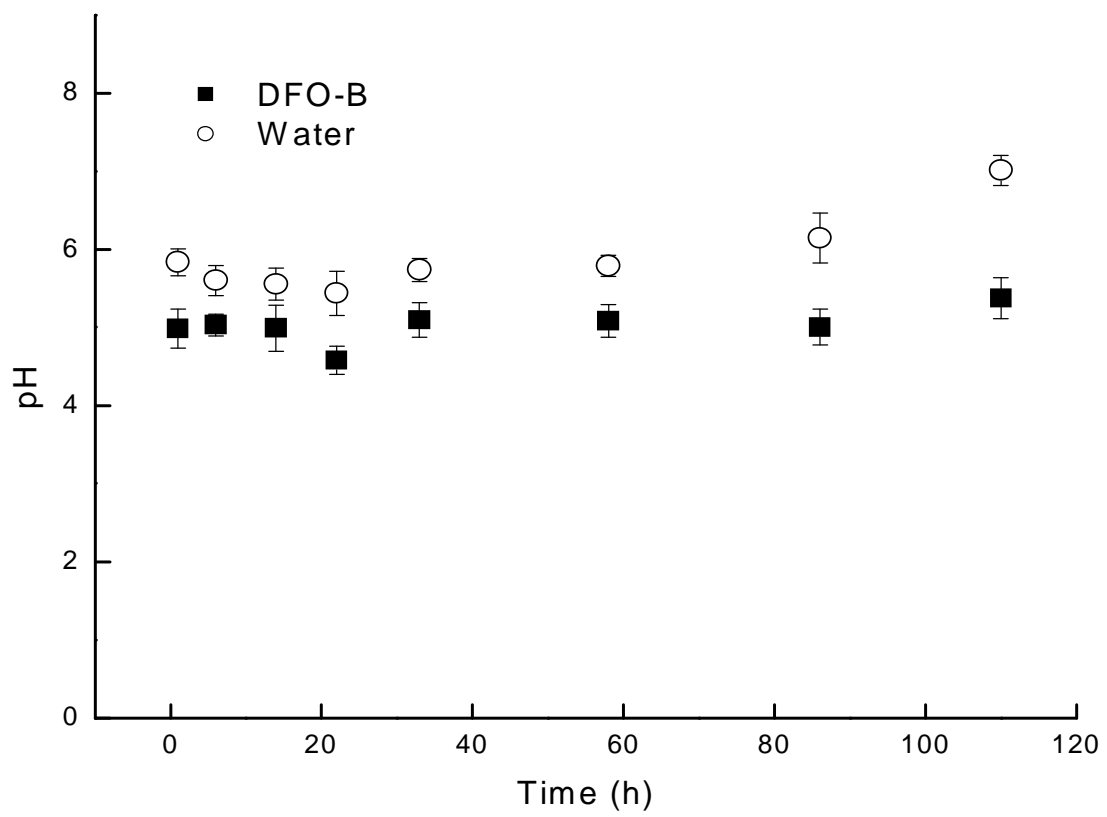


Figure 10. Variations of pH during the reaction between 1 g L⁻¹ galena and 200 μM.

REFERENCES

- Baes C. F. and Mesmer R. E. (1976). *The hydrolysis of cations*. Krieger Publishing Company, Malabar, FL, 489 pp.
- Bottomley D. J. (1984) Origins of some arseniferous groundwater in Nova Scotia and New Brunswick. *Can. J. Hydrol.* **69**, 223–257.
- Brown G. E. Jr., Foster A. L., and Ostergren J. D. (1999) Mineral surfaces and bioavailability of heavy metals: A molecular-scale perspective. *Proc. Natl. Acad. Sci. USA.* **96**, 3388–3395.
- Craw D. and Pacheco L. (2002) Mobilization and bioavailability of arsenic around mesothermal gold deposits in a semiarid environment, Otago, New Zealand. *Sci. World. J.* **2**, 308-319.
- Cervini-Silva J. and Sposito G. (2002) Steady-State Dissolution Kinetics of Aluminum-Goethite in the Presence of Desferrioxamine-B and Oxalate Ligands. *Environ. Sci. Technol.* **36**, 337-342.
- Cheah S. F., Kraemer S. M., Cervini-Silva J. and Sposito G. (2003) Steady-state dissolution kinetics of goethite in the presence of desferrioxamine B and oxalate ligands: implications for the microbial acquisition of iron. *Chem. Geol.* **198**, 63– 75.
- Chen C. J., Chuang Y. C., Lin T. M., and Wu H. Y. (1985) A retrospective study on malignant neoplasms of bladder, lung and liver in blackfoot disease endemic area in Taiwan. *Cancer Res.* **45**, 5895–5899.
- Cocozza C., Tsao C. C. G., Cheah S. F., Kraemer S. M., Raymond K. N., Miano T. M. and Sposito G. (2002) Temperature dependence of goethite dissolution promoted by trihydroxamate siderophores. *Geochim. Cosmochim. Acta* **66**, 431–438.
- Cornell R. M. and Schwertmann U. (2003) *The Iron Oxides. Structure, Properties, Reactions, Occurrences and Uses*, VCH Publishers: Weinheim.

Craw D., Falconer D. and Youngson J. H. (2003) Environmental arsenopyrite stability and dissolution: theory, experiment, and field observations. *Chem. Geol.* **199**, 71-82.

Craw D. and Pacheco L. (2002) Mobilization and bioavailability of arsenic around mesothermal gold deposits in a semiarid environment, Otago, New Zealand. *Sci. World. J.* **2**, 308-319.

Cruz R., Lazaro I., Rodriguez J. M., Monroy M., and Gonzalez I. (1997) Surface characterization of arsenopyrite in acidic medium by triangular scan voltammetry on carbon paste electrodes. *Hydrometallurgy* **46**, 303-319.

De Giudici G., Rossi A., Fanfani L., and Lattanzi P. (2005) Mechanisms of galena dissolution in oxygen-saturated solutions : Evaluation of pH effect on apparent activation energies and mineral-water interface. *Geochim. Cosmochim. Acta* **69**, 2321-2331.

De Giudici G., Ricci P., Lattanzi P., and Anedda A. (2007) Dissolution of the (001) surface of galena: An *in situ* assessment of surface speciation by fluid-cell micro-Raman spectroscopy. *Amer. Mineral.*, **92**, 518-524.

Elrick, K. A. and Horowitz A. J. (1986) Analysis of rocks and sediments for arsenic, antimony, and selenium, by wet digestion and hydride generation atomic absorption. Varian Instruments at Work. Number AA-56, 5 pp.

Frost R. R. and Griffin R. A. (1977) Effect of pH on adsorption of arsenic and selenium from landfill leachate by clay minerals. *Soil Sci. Soc. Am. J.* **41**, 53-57.

Georgiadis M., Cai Y. and Solo-Gabriele H. M. (2006) Extraction of arsenate and arsenite species from soils and sediments. *Environ. Poll.* **141**, 22-29.

Goldhaber, M. B. (1983) Experimental study of metastable sulfur oxyanion formation during pyrite oxidation at pH 6-9 and 30 °C. *Am. J. Sci.* **283**, 193-217.

Greenwood N. N. and Earnshaw A. (1984) *Chemistry of the Elements*. Pergamon Press, Oxford.

Haack E., Johnston C. T. and Maurice P. A. (2006) In Proceedings of the 232nd National Meeting of The American Chemical Society, *The American Chemical Society*: San Francisco, CA, September 10-14.

Hernlem, B. J., Vane, L. M. and Sayles, G. D. (1995) Stability constants for complexes of the siderophore desferrioxamine B with selected heavy metal cations. *Inorg. Chim. Acta* **244**, 179-184.

Hernlem B. J., Vane L. M. and Sayles G. D. (1999) The application of siderophores for metal recovery and waste remediation: examination of correlations for prediction of metal affinities. *Water Res.* **33**, 951-960.

Hersman L., Lloyd T. and Sposito G. (1995) Siderophore-promoted dissolution of hematite. *Geochim. Cosmochim. Acta* **59**, 3327-3330.

Holmén B. A. and Casey W. H. (1996) Hydroxamate ligands, surface chemistry, and the mechanism of ligand-promoted dissolution of goethite [α -FeOOH(s)]. *Geochim. Cosmochim. Acta* **60**, 4403-4416.

Holmén B. A., Sison J. D., Nelson D. C. and Casey W. H. (1999) Hydroxamate siderophores, cell growth and Fe(III) cycling in two anaerobic iron oxide media containing *Geobacter metallireducens*. *Geochim. Cosmochim. Acta* **63**, 227-239.

Kalinowski B. E., Liermann L. J., Givens S. and Brantley S. L. (2000) Rates of bacteria-promoted solubilization of Fe from minerals: a review of problems and approaches. *Chem. Geol.* **169**, 357-370.

Kiss, T. y Farkas, E. (1998) Metal-binding Ability of Desferrioxamine B. *Journal of Inclusion Phenomena and Molecular Recognition in Chemistry*. **32**, 385-403.

Korte N. C. and Fernando Q. (1991) A Review of Arsenic(III) in Groundwater. *Crit. Rev. Environ. Control.* **21**, 1-39.

Kraemer S. M., Cheah S. F., Zapf R., Xu J., Raymond K.N. and Sposito G. (1999). Effect of hydroxamate siderophores on Pb(II) adsorption and Fe release by goethite. *Geochim. Cosmochim. Acta* **63**, 3003– 3008.

Kraemer S. M., Xu J., Raymond K. and Sposito G. (2002). Adsorption of Pb(II) and Eu(III) by Oxide Minerals in the Presence of Natural and Synthetic Hydroxamate Siderophores. *Environ. Sci. Technol.*, **36**, 1287-1291.

Kraemer S. M., Butler A., Borer P. and Cervini-Silva J. (2005) Biogenic ligands and the dissolution of iron bearing minerals in marine systems. *Rev. Mineral. Geochem.* **59**, 53-84.

Lengke M. F. and Tempel R. N. (2002) Reaction rates of natural orpiment oxidation at 25 to 40°C and pH 6.8 to 8.2 and comparison with amorphous As₂S₃ oxidation. *Geochim. Cosmochim. Acta* **66**(18), 3281–3291.

Liermann L. J., Kalinowski B. E., Brantley S. L. and Ferry J. G. (2000) Role of bacterial siderophores in dissolution of hornblende. *Geochim. Cosmochim. Acta* **64**, 587–602.

Martell A. E., Smith R. M. and Motekaitis R. J. *Critically Stability Constants Database*. NIST Vol. 2 Gaithersburg, MD, 1995.

Maurice P. A., Lee Y. J. and Hersman L. E. (2000) Dissolution of Al-substituted goethites by an aerobic *Pseudomonas mendocina* var. *Geochim. Cosmochim. Acta* **64**, 1363-1374.

Maurice P. A., Vierkorn M. A., Hersman L. E. and Fulghum J. E. (2001) Dissolution of well and poorly ordered kaolinites by an aerobic bacterium. *Chem. Geol.* **180**, 81-97.

McKibben, M. A. and Barnes, H. L. (1986). Oxidation of pyrite in low temperature acidic solutions: Rate laws and surface textures. *Geochim. Cosmochim. Acta*. **50**, 1509-1520.

Merian E. (1991) *Metals and their compounds in the environment. Occurrence, analysis and biological relevance*. VCH publishers, Germany, pp. 87-93.

Moffett J. (1988) The determination of arsenic in non-silicate geological ore samples using a vapor generation accessory. *Varian Instruments at Work*. Number AA-78, 4p.

Monroy-Fernandez M. G., Mustin C., de Donato P., Barres O., Marion P. and Berthelin J. (1995) Occurrences at mineral-bacteria interface during oxidation of arsenopyrite by *Thiobacillus ferrooxidans*. *Biotechnol. Bioengin.* **46**, 13-21.

Moses, C. O., Nordstrom, D. K., Herman, J. S. and Mills, A. L. (1987). Aqueous pyrite oxidation by dissolved oxygen and by ferric iron. *Geochim. Cosmochim. Acta.* **51**, 1561-1571.

Ng J. C., Wang J. and Shraim A. (2003) A global health problem caused by arsenic from natural sources. *Chemosphere* **52**, 1353-1359.

Nordstrom, D. K. and Archer D. G. (2003) *Arsenic in Ground Water: Geochemistry and Occurrence* (eds Welch A. H., Stollenwerk K. G.). Kluwer Academic Publishers, Boston, pp. 1-25.

O'Day P., Vlassopoulos D., Meng X. and Benning L. G. (eds) (2005) Advances in Arsenic Research: Integration of Experimental and Observational Studies and Implications for Mitigation. ACS Symposium Series No. 915, American Chemical Society, 450 pp.

Palache C., Berman H. and Frondel C. (1944) The system of mineralogy of James Dwight Dana and Edward Salisbury Dana, vol. 1. *Elements, sulfides, sulfosalts, oxides*. 7th ed. John Wiley, London, 1872pp.

Parkhurst D. L. (1995) User's guide to PHREEQC-A computer program for speciation, reaction-path, advective-transport, and inverse geochemical calculations. *USGS Water Resources Investigations Report*, 95-4227.

Pinto S. S. and Nelson K. W. (1976) Arsenic toxicology and industrial exposure. *Annu. Rev. Pharmacol. Toxicol.* **16**, 95-100.

Plant J. A., Kinniburgh D. G., Smedley P. L., Fordyce F. M. and Klinck B. A. (2005) Arsenic and selenium. In *Environmental*

Geochemistry: Treatise on geochemistry (ed. L. B. Sherwood). British Geological survey, Nottingham, UK.

Rodríguez V. M., Jiménez-Capdeville M. E. and Giordano M. (2003) The effects of arsenic exposure on the nervous system. *Toxicol. Lett.* **145**, 1-18

Rohwerder T., Gehrke T., Kinzler K. and Sand W. (2003) Bioleaching review part A: progress in bioleaching: fundamentals and mechanisms of bacterial metal sulfide oxidation. *Appl. Microbiol. Biotechnol.* **63**, 239–248

Smith A. H., Lopiperom P. A., Bates M. N., and Steinmaus C. M. (2002) Arsenic epidemiology and drinking water standards. *Science* **296**, 2145–2146.

Solinas V. (1994) Cation effects on the adsorption of desferrioxamine B (DFOB) by humic acid. In: *Humic Substances in the Global Environment and Implications on Human Health* (eds. N. Senesi and T. M. Miano). Elsevier: Amsterdam. pp. 1183–1188.

Steudel R. (1996) Mechanism for the formation of elemental sulfur from aqueous sulfide in chemical and microbiological desulfurization processes. *Ind. Eng. Chem. Res.* **35**, 1417–1423.

Stumm W. and Morgan J. J. (1996) *Aquatic Chemistry: Chemical Equilibria and Rates in Natural Waters*, Wiley, New York. 1040 pp.

Telford J. R. and Raymond K. N. (1996) Siderophores. In: J. E. Atwood, J. E. Davis, D. D. MacNicol and F. Vögtle (Eds.), *Comprehensive Supramolecular Chemistry* Vol. 1., Elsevier, Oxford. 245pp.

Voigt D. E., Brantley S. L. and Hennet R. J. C. (1996) Chemical fixation of arsenic in contaminated soils. *Appl. Geochem.* **11**, 633–643.

Walker F. P., Schreiber M. E., and Rimstidt, J. D. (2006) Kinetics of arsenopyrite oxidative dissolution by oxygen. *Geochim. Cosmochim. Acta* **70**, 1668-1676.

Wandersman, C. and Delepelaire, P. (2004) Bacterial Iron Sources: From Siderophores to Hemophores. *Annu. Rev. Microbiol.* **58**, 611-647.

Watteau F. and Berthelin J. (1994) Microbial dissolution of iron and aluminum from soil minerals: efficiency and specificity of hydroxamate siderophores compared to aliphatic acids. *Eur. J. Soil Biol.* **30**, 1 -9.

Zhang H., Penn R. L., Hamers, R. J., Banfield J. F. (1999) Enhanced adsorption of molecules on the surface of nanocrystalline particles. *J. Phys. Chem. B.* **103**, 4656-4662.